SOVIET PHYSICS USPEKHI VOLUME 4, NUMBER 3 NOVEMBER-DECEMBER 1962

APPLICATION OF PARAMAGNETIC CRYSTALS IN QUANTUM ELECTRONICS

G. M. ZVEREV, N. V. KARLOV, L. S. KORNIENKO, A. A. MANENKOV, and A. M. PROKHOROV

Usp. Fiz. Nauk 77, 61-108 (May, 1962)

CONTENTS

I. INTRODUCTION

UNTIL very recently, electronic devices represented the only means for producing monochromatic electromagnetic waves. Electronic devices can be used to generate monochromatic radiation up to the ultramicrowave region and provide an extremely high spectral energy density. To obtain the same spectral energy density from a black body it would be necessary to heat the black body to a temperature of 10^{14}—10^{20} deg.

In the optical region, however, the sources that have been available until the present provide a spectral energy density corresponding to temperatures of several thousand degrees. The lack of optical radiation sources with high spectral densities has been a stumbling block in the solution of a number of important scientific and technological problems. The first optical sources with high radiation densities are now beginning to appear. The technology of monochromatic optical generators represents a fusion of the techniques of optical spectroscopy and microwave spectroscopy.

Monochromatic optical generators have become possible as a result of the development of a new field of science—quantum electronics.

The first development in this new field was the building of the first quantum-mechanical device—the maser (1954—1955). The working material in this device is a beam of ammonia molecules. This oscillator is characterized by a high frequency stability and a high degree of monochromaticity and is being used for both scientific and technical purposes because of these desirable properties.

The first molecular, or paramagnetic, amplifiers were built in 1957—1958; in these devices the working material is a paramagnetic crystal. Because the natural noise level in these amplifiers is so low they have improved receiver sensitivity a hundred-fold in the centimeter and decimeter wavelength ranges.

The basis of the operation of quantum-mechanical oscillators and amplifiers (masers) is the ability of molecules in an excited state to release energy when triggered by incident radiation. The photons emitted by the molecules are identical with the photons of the primary radiation. If a maser is to amplify incident radiation, thermodynamic equilibrium of the molecular system must be disturbed in such a way that the number of particles in an upper level is greater than in a lower level. This situation can be described by saying that the molecular system is in a negative temperature state. A number of means are presently being employed to produce negative temperatures in atomic and molecular systems. This field has been reviewed in several papers;[1-5] the problems associated with the design of maser amplifiers and oscillators in the infrared and optical regions are discussed in [5].

The present review is concerned with the use of paramagnetic crystals in microwave and optical maser devices in which negative temperatures are achieved by means of auxiliary or "pump" radiation.

II. ENERGY LEVELS OF PARAMAGNETIC IONS IN CRYSTALS

The basis of quantum-mechanical centimeter and decimeter devices in which the working material is a paramagnetic crystal is the phenomenon known as electron paramagnetic resonance (EPR), discovered by E. K. Zavoĭskii in 1944.[6] This effect can be observed in a system of particles with nonvanishing electron spin if the spin is not cancelled by chemical binding of the particle in its environment. In particular, the effect is prevalent in crystals which contain ions of the transition groups; these are the subject of the present paper. Elements of the transition groups are characterized by the fact that filling of the outer electronic shells starts before the inner shell is completely filled. Examples of such unfilled shells are the nd and nf shells for $n \geq 3$. The iron group consists of elements with an unfilled 3d shell while the rare-earth group consists of elements with an unfilled 4f shell. The elements in these groups have been investigated quite extensively. The other transition groups, palladium, platinum, and uranium, in which the unfilled

shells are 4d, 5d, and 5f respectively, have not been investigated as extensively.

We shall be interested only in crystals in which the isolated paramagnetic ions, i.e., ions having uncompensated spins (and corresponding magnetic moments), interact weakly with each other. In such crystals the paramagnetic ions represent a relatively small impurity that replaces isomorphically certain diamagnetic ions of which the crystal lattice is constructed.

The energy levels of a free ion having a resultant angular momentum J in a fixed magnetic field are given by the expression

$$W = g\beta HM, \tag{1}$$

where M is the component of J in the direction of the magnetic field, and takes on values from +J to −J; g is the Lande g factor for the free ion, and $\beta = eh/4\pi mc$ is the Bohr magneton. If a perpendicular alternating magnetic field of frequency ν is applied together with the field H, magnetic dipole transitions will be induced between the ion energy levels; only those transitions are allowed for which $|\Delta M| = 1$. The resonance conditions are satisfied when the value of the fixed magnetic field H and the frequency of the alternating field ν satisfy the relation

$$h\nu = g\beta H. \tag{2}$$

In a crystal a paramagnetic ion can no longer be regarded as free inasmuch as it is subject to the electric field produced by neighboring ions (we shall be interested chiefly in ionic crystals). To a good degree of approximation this field can be regarded as static. As in the Stark effect in atomic spectroscopy, the energy levels of the free ion are split into several components by the crystalline field. The number of components and the magnitude of the splitting depend on the symmetry and strength of the crystalline field in which the paramagnetic ion is located.

An estimate of the strength of the crystalline field can be obtained by comparing its effect on the ion with the internal interactions characteristic of the free ion; these internal effects are the spin-orbit interaction and the Coulomb interaction between the electrons. These effects are responsible for the magnetic properties of ions of the various transition groups.

Three cases are usually considered: these are called respectively the weak-field case, the intermediate-field case, and the strong-field case. Weak crystalline fields are characteristic of paramagnetic crystals containing ions with unfilled 4f and 5f shells, that is to say, ions of the rare earths and uranium. In these cases the magnetic f electrons lie rather deep in the ion and are well shielded from the effect of the crystalline field by the outer electronic shells. Under these conditions the effect of the crystalline field is weaker than that due to the spin-orbit coupling and the Coulomb interaction between electrons.

Intermediate crystalline fields are found in ions of the iron group. The magnetic 3d electrons are located in the outer shell and the interaction with the crystalline field is stronger than the spin-orbit coupling, but weaker than the Coulomb interaction of electrons in the ion.

In ions of the palladium and platinum group, in which strong crystalline fields appear, the effect of the crystalline field on the outer 4d and 5d electrons is comparable with the Coulomb interaction between electrons. A similar picture obtains in the cyanide complexes formed by elements of the iron group.

The total Hamiltonian for an ion subject to the crystalline field and an external magnetic field can be written as a sum of terms:

$$\hat{\mathcal{H}} = \hat{\mathcal{H}}_F + \hat{\mathcal{H}}_V + \hat{\mathcal{H}}_{LS} + \hat{\mathcal{H}}_{SS} + \hat{\mathcal{H}}_N + \beta\mathbf{H}(\hat{\mathbf{L}} + 2\hat{\mathbf{S}}) - g_N\beta_N\mathbf{H}\hat{\mathbf{I}}, \tag{3}$$

where $\hat{\mathcal{H}}_F$ is the energy of the free ion; $\hat{\mathcal{H}}_V$ is the electrostatic energy in the field produced by the neighboring ions in the crystal; $\hat{\mathcal{H}}_{LS}$ is the energy of the spin-orbit interaction; $\hat{\mathcal{H}}_{SS}$ is the energy of the spin-spin interaction of electrons in the ion; $\hat{\mathcal{H}}_N$ is the energy associated with interaction between the electronic shell of the ion and the nucleus (if the latter has a magnetic dipole moment or an electric quadrupole moment); $\beta\mathbf{H}(\hat{\mathbf{L}} + 2\hat{\mathbf{S}} - g_N\beta_N\mathbf{H}\cdot\hat{\mathbf{I}})$ is the energy of the interaction of the electrons and nucleus with the external magnetic field (β and β_N are the electronic and nuclear Bohr magnetons, H is the applied external magnetic field, $\hat{\mathbf{L}}$ and $\hat{\mathbf{S}}$ are the orbital moment and the spin of the electronic shell, g_N is the nuclear gyromagnetic ratio, and I is the nuclear spin). In the iron group the splittings due to the various interactions are of the following orders of magnitude:

$$\hat{\mathcal{H}}_F \sim 10^5\,\text{cm}^{-1},\ \hat{\mathcal{H}}_V \sim 10^3 - 10^4\,\text{cm}^{-1},\ \hat{\mathcal{H}}_{LS} \sim 10^2\,\text{cm}^{-1},$$
$$\hat{\mathcal{H}}_{SS} \sim 1\,\text{cm}^{-1},\ \hat{\mathcal{H}}_N \sim 10^{-2}\,\text{cm}^{-1}.$$

In an external field of order 10^4 Oe, we find that $\beta\mathbf{H}(\hat{\mathbf{L}} + 2\hat{\mathbf{S}})$ is about one cm^{-1} while $g_N\beta_N\mathbf{H}\cdot\hat{\mathbf{I}}$ is about $10^{-3}\ \text{cm}^{-1}$.

The electron paramagnetic resonance method can only be used to study the lower levels of a paramagnetic ion, which are appreciably populated at room temperature or lower; these levels are tens or hundreds of wavenumbers above the lowest level. The level structure depends on the particular ion as well as the strength and symmetry of the crystalline field.

For this reason the higher energy levels, associated with $\hat{\mathcal{H}}_F$, are usually not considered since they have a negligible effect on the positions of the levels in the lower group. An exception occurs in ions whose ground state is an S state (L = 0). In this case the only splitting of the ground state is due to admixtures of the higher states of $\hat{\mathcal{H}}_F$. The behavior of the lowest energy levels is usually described by a reduced Hamil-

tonian known as the spin Hamiltonian.[7] By using the spin Hamiltonian it is possible to avoid a detailed analysis of the effect of various interactions on the structure of the lower energy levels and the corresponding states. This group of electronic states is characterized by the single quantum number S′, although each state is actually a complex mixture of spin and orbital states of the free ion. The number S′ is called the effective spin and is determined by averaging over the $(2S' + 1)$ energy levels in the lowest group. The quantity S′ may, or may not, coincide with the true spin of the ion S.

When the notion of an effective spin is used one assumes that the $(2S' + 1)$ energy levels correspond to different orientations of a magnetic dipole in the applied magnetic field. However the effective magnetic moment of this dipole may not correspond to the "pure" spin value. This lack of correspondence is taken into account by the introduction of a spectroscopic splitting factor g, which can differ from the g factor for the free spin (2.00229). The energy levels of the effective spin can be split in the absence of a magnetic field. The presence of this splitting, called the zero-field splitting, means that in addition to containing terms that describe the interaction of the dipole with the external magnetic field, the spin Hamiltonian also contains terms that express, say, the interaction between the magnetic electrons and the crystalline field; this is possible by virtue of the spin-orbit coupling and other interactions.

In this review we limit ourselves to these very general remarks concerning electron paramagnetic resonance; the reader who is interested can refer to a number of monographs devoted to this subject.[8-12]

Quantum-mechanical amplifiers for the infrared and optical regions make use of transitions to higher energy levels of paramagnetic ions in crystals.

Information concerning these levels can be obtained by conventional spectroscopic techniques.

The absorption spectra of paramagnetic crystals exhibit a great deal of variety and depend on both the nature of the paramagnetic ion and the crystalline environment.

Ions of the iron group located in a crystal lattice of cubic symmetry (or a lattice that is approximately cubic) have several wide absorption bands in the visible, corresponding to transitions between levels of the same spin multiplet. In addition, there are frequently weak narrow lines corresponding to transitions between levels of different multiplicity. The position of the band is not related to the terms of the free ion.

Ions of the rare-earth elements usually exhibit narrow lines in the infrared and visible; these correspond approximately to transitions between terms of the free ion. Many ions of the rare earth group are fluorescent (Eu^{2+}, Gd^{3+}, Tb^{3+}, Sm^{3+} etc.).

The difference between the optical spectra of ions in the different transition groups arises because, as noted above, the interaction between the rare-earth ions and the crystalline field is weak whereas the interaction of the crystalline field with ions of the iron group is of intermediate strength.

Calculations of level splitting for paramagnetic ions in crystals were carried out a long time ago in connection with the interpretation of the paramagnetic susceptibility of crystals containing ions of the iron group.[13-15] In recent years this work has been carried further in connection with investigations of paramagnetic resonance and optical spectra in crystals containing ions of various transition groups.[11,16-18] The optical transitions observed in paramagnetic crystals usually connect levels of the same parity. For this reason electric dipole transitions are strongly forbidden. Magnetic dipole transitions, however, are observed in certain rare-earth ions. The ions of the iron group usually exhibit electric dipole transitions. In this case the forbiddeness is partially relaxed because the crystalline field is noncentral, because of the dynamic distortion of the crystalline field, or because of the covalent bond of the paramagnetic ion with the surrounding ions in the lattice. The data that have been obtained in work on optical absorption spectra and fluorescent spectra of paramagnetic crystals have made it possible to extend the principles of quantum electronics to the optical region and have been instrumental in the operation of the first solid-state optical masers.

Typical paramagnetic crystals. We now consider certain paramagnetic crystals that have found practical application in paramagnetic amplifiers and oscillators.

The most widely used working material in microwave paramagnetic amplifiers is ruby. Ruby is a crystallographic modification of aluminum oxide (Al_2O_3) in which some of the Al^{3+} ions are isomorphically replaced by Cr^{3+} ions.

The Cr^{3+} ion has three electrons in the unfilled 3d shell. In the ruby crystal the chromium ion is surrounded by 6 oxygen ions; these produce an electric field having a strong component with cubic symmetry and a much weaker component with trigonal symmetry. The cubic component of the crystalline field splits the ^4F ground level of the ion, which has a sevenfold orbital degeneracy, into two triplets and a singlet; the singlet has the lowest energy. The next (triplet) level is approximately 10^4 cm^{-1} higher. Under the effect of the trigonal crystalline field and the spin-orbit coupling the fourfold spin degeneracy of the ground state corresponding to the spin value $S = 3/2$ is removed and two Kramers doublets with small (approximately 0.4 cm^{-1}) zero-field splitting are formed. The remaining double Kramers degeneracy of each level is removed by the application of the external magnetic field.

The behavior of the lowest group of four spin levels as a function of the strength of the applied external

magnetic field and its direction (with respect to the trigonal axis of the crystal) can be described by the spin Hamiltonian

$$\hat{\mathcal{H}} = g_{\parallel}\beta H_z \hat{S}_z + g_{\perp}\beta (H_x \hat{S}_x + H_y \hat{S}_y) + D\left[\hat{S}_z^2 - \frac{1}{3}S(S+1)\right]. \quad (4)$$

Here, $g_{||}$ and $g_{\perp}$ are the g factors in the directions parallel and perpendicular to the trigonal axis of the crystal; β is the Bohr magneton; $\hat{S}_X$, $\hat{S}_y$, and $\hat{S}_Z$ are the operators associated with the projections of the electronic spin ($S = 3/2$) on the corresponding axes of the coordinate system (the z axis is along the trigonal axis); H_X, H_y, and H_Z are the projections of the external magnetic field **H** on these axes and D is the constant that characterizes the trigonal crystalline field.

A number of workers have determined the values of the constants appearing in the spin Hamiltonian.[19-23] The latest measurements[23] yielded

$$g_{\parallel} = 1.9840 \pm 0.0006,$$
$$g_{\perp} = 1.9867 \pm 0.0006,$$
$$D = -0.3831 \pm 0.0002\ \text{cm}^{-1}.$$

We can assume without loss of generality that the magnetic field **H** is in the xz plane ($H_y = 0$). To simplify the calculations we also assume that $g_{||} = g_{\perp} = g$. Using the notation $g\beta H_{X,Z}/|D| = h_{X,Z}$ we write (4) in the form

$$\hat{\mathcal{H}}' = -\left(\hat{S}_z^2 - \frac{5}{4}\right) + h(\cos\theta \cdot \hat{S}_z + \sin\theta \cdot \hat{S}_x), \quad (4a)$$

where θ is the angle between the external magnetic field and the trigonal axis of the crystal and $h = \sqrt{h_X^2 + h_Z^2}$. The eigenvalues of (4), E_i, are related to the eigenvalues of (4a), ϵ_i, by the expression

$$E_i = |D|\varepsilon_i. \quad (5)$$

To find the energy eigenvalues we must determine the matrix elements of the Hamiltonian (4a) and solve the secular equation, which is given by the determinant

$$\begin{vmatrix} a_{11}-\varepsilon & a_{12} & 0 & 0 \\ a_{21} & a_{22}-\varepsilon & a_{23} & 0 \\ 0 & a_{32} & a_{33}-\varepsilon & a_{34} \\ 0 & 0 & a_{43} & a_{44}-\varepsilon \end{vmatrix} = 0, \quad (4b)$$

where

$$a_{11} = -1 - (3/2)h\cos\theta,$$
$$a_{22} = 1 - (1/2)h\cos\theta,$$
$$a_{33} = 1 + (1/2)h\cos\theta,$$
$$a_{44} = -1 + (3/2)h\cos\theta,$$
$$a_{12} = a_{21} = a_{34} = a_{43} = (\sqrt{3}/2)h\sin\theta,$$
$$a_{32} = a_{23} = h\sin\theta.$$

The wave functions used as a basis are the eigenfunctions of the operator $\hat{S}_Z$, and the subscripts 1, 2, 3, and 4 refer to the eigenvalues of this operator M = $-3/2$, $-1/2$, $1/2$, $3/2$. From (4) we obtain a fourth-order equation for the eigenvalues of the operator in (4a):

$$\varepsilon^4 - \varepsilon^2(2 + 2{,}5h^2) + 2\varepsilon h^2(3\cos^2\theta - 1) + \frac{9}{16}h^4 - \frac{h^2}{2}(6\cos^2\theta - 1) + 1 = 0. \quad (6)$$

This equation is biquadratic in h:

$$h^4 - 2ah^2 + b = 0, \quad (6a)$$

where

$$a = a_1 + a_2\cos^2\theta,$$
$$a_1 = (4/9)(5\varepsilon^2 + 4\varepsilon - 1),$$
$$a_2 = (8/3)(1 - 2\varepsilon),$$
$$b = (16/9)(\varepsilon^2 - 1)^2.$$

Solving (6) we can determine the value of h as a function of ϵ for different values of θ. In Figs. 1–3 we show ϵ as a function of h for θ equal to 0°, 54°44′, and 90°. We note that the curves in Fig. 2 are symmetric with respect to the abscissa axis.

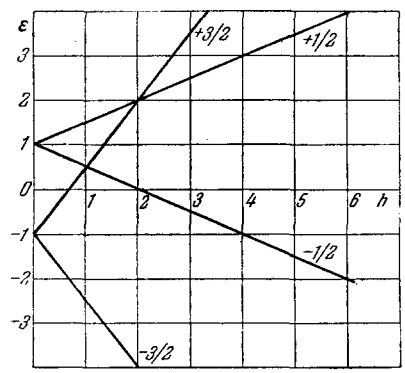

FIG. 1. Energy levels of the Cr^{3+} ion in corundum ($\theta = 0°$).

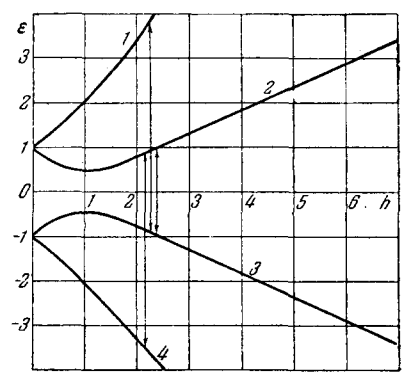

FIG. 2. Energy levels of the Cr^{3+} ion in corundum ($\theta = 54°44'$).

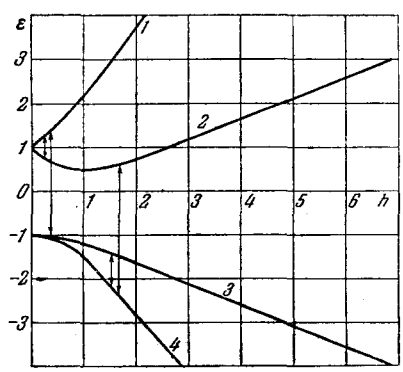

FIG. 3. Energy levels of the Cr^{3+} ion in corundum ($\theta = 90°$).

The design of quantum-mechanical amplifiers requires a knowledge of the probability of induced transitions between various levels in addition to a knowledge of the energy-level structure. The probability of an induced transition between two levels j and k is proportional to the square of the matrix element of the operator $\mathbf{H}_1\hat{\boldsymbol{\mu}}$ (where $\mathbf{H}_1$ is the vector associated with the high-frequency magnetic field and $\hat{\boldsymbol{\mu}} = g\beta\hat{\mathbf{S}}$ is the magnetic moment of the ion) and can be written in the form

$$W_{jk} = \frac{4\pi^2}{h^2}|\langle j|\mathbf{H}_1\boldsymbol{\mu}|k\rangle|^2 g(\nu) = \frac{4\pi^2 g^2\beta^2}{h^2}|\langle j|\mathbf{H}_1\hat{\mathbf{S}}|k\rangle|^2 g(\nu), \quad (7)$$

where $g(\nu)$ is the shape factor of the line $\left(\int_0^\infty g(\nu)\,d\nu = 1\right)$. Thus,

$$W_{jk} \sim |\langle j|\mathbf{H}_1\hat{\mathbf{S}}|k\rangle|^2 = |H_{1x}\langle j|\hat{S}_x|k\rangle + H_{1z}\langle j|\hat{S}_z|k\rangle|^2 + |H_{1y}\langle j|\hat{S}_y|k\rangle|^2, \quad (8)$$

where

$$\langle j|\hat{S}_z|k\rangle = -\frac{3}{2}c_{j1}^*c_{k1} - \frac{1}{2}c_{j2}^*c_{k2} + \frac{1}{2}c_{j3}^*c_{k3} + \frac{3}{2}c_{j4}^*c_{k4},$$

$$\langle j|\hat{S}_x|k\rangle = \frac{\sqrt{3}}{2}(c_{j1}^*c_{k2} + c_{j2}^*c_{k1} + c_{j3}^*c_{k4} + c_{j4}^*c_{k3}) + c_{j2}^*c_{k3} + c_{j3}^*c_{k2},$$

$$\langle j|\hat{S}_y|k\rangle = i\frac{\sqrt{3}}{2}(c_{j1}^*c_{k2} - c_{j2}^*c_{k1} + c_{j3}^*c_{k4} - c_{j4}^*c_{k3}) + i(c_{j2}^*c_{k3} - c_{j3}^*c_{k2}).$$

The quantity c_{mn} is the coefficient in the expansion of the state $|m\rangle$, corresponding to the energy level ϵ_m, in eigenfunctions of the operator $\hat{S}_z$.

A knowledge of the probabilities of the induced transitions allows us to clarify the degree of forbiddeness of the transitions corresponding to the primary and pump radiation and to find the optimum position of the working material in the cavity resonator or slow-wave system of the paramagnetic amplifier. Another material used in paramagnetic amplifiers is corundum with the impurity Fe^{3+}.

The Fe^{3+} ion has five electrons in its unfilled 3d shell and the ground state is a ^6S state. Thus, the ground state of this ion does not exhibit orbital degeneracy (L = 0). The results of experiments with different crystallographic compounds containing the Fe^{3+} ion as an isomorphic substitution have shown that the sixfold spin degeneracy of the ground state is partially removed in the crystalline fields. The ground-state splitting is explained by assuming that the ground state of the ion is no longer pure in the crystalline field, but contains an admixture of the higher energy states (for which $L \neq 0$).

The EPR spectrum of the Fe^{3+} ion in corundum can be described by the spin Hamiltonian

$$\hat{\mathcal{H}} = g\beta\mathbf{H}\hat{\mathbf{S}} + D\left[\hat{S}_z^2 - \frac{1}{3}S(S+1)\right] + \frac{a}{6}\left[\hat{S}_\xi^4 + \hat{S}_\eta^4 + \hat{S}_\zeta^4 - \frac{1}{5}S(S+1)(3S^2+3S-1)\right] + \frac{F}{180}[35\hat{S}_z^4 - 30S(S+1)\hat{S}_z^2 + 25\hat{S}_z^2 - 6S(S+1) + 3S^2(S+1)^2]. \quad (9)$$

Here we have used the same notation as in (4). The spectroscopic splitting factor, g, is isotropic. The trigonal crystalline field is characterized by the two constants D, and F, while a is the constant that characterizes the cubic field. As in the preceding case, the z axis is along the trigonal axis, which is the (111) axis of the coordinate system ξ, η, ζ constructed on the cubic axes of the crystalline field; $S = 5/2$. Electron paramagnetic resonance of the Fe^{3+} ion in corundum has been studied by a number of workers.[24-27] The constants in the spin Hamiltonian are found to be functions of the temperature and Fe^{3+} concentration. At 4.2°K, with a paramagnetic-ion concentration of the order of 10^{-2}%, these constants are:[27]

$$g = 2.0029 \pm 0.0007, \quad D = (+1719.2 \pm 0.6)\cdot 10^{-4}\ \text{cm}^{-1},$$
$$a - F = (+339.2 \pm 0.6)\cdot 10^{-4}\ \text{cm}^{-1}, \quad |a| = (237 \pm 1)\cdot 10^{-4}\ \text{cm}^{-1}.$$

The Fe^{3+} ions in the corundum lattice form two nonequivalent systems so that the observed EPR spectrum consists of two different systems of paramagnetic absorption lines. However, at a given angle θ between the external magnetic field and the trigonal axis of the crystal the two spectra can be made to coincide by rotation about the trigonal axis. In this case, which is of practical importance, the equality of the energy eigenvalues and the eigenfunctions can be obtained from the matrix associated with a Hamiltonian of the form:

$$\hat{\mathcal{H}} = \begin{vmatrix} a_{11} & a_{12} & 0 & a_{14} & 0 & 0 \\ a_{21} & a_{22} & a_{23} & 0 & 0 & 0 \\ 0 & a_{32} & a_{33} & a_{34} & 0 & a_{36} \\ a_{41} & 0 & a_{43} & a_{44} & a_{45} & 0 \\ 0 & 0 & 0 & a_{54} & a_{55} & a_{56} \\ 0 & 0 & a_{63} & 0 & a_{65} & a_{66} \end{vmatrix}, \quad (10)$$

where

$$a_{11} = -\left(\frac{5}{2}\right)h_z + 5 - \left(\frac{1}{3}\right)(\alpha - f),$$
$$a_{22} = -\left(\frac{3}{2}\right)h_z + 1 + (\alpha - f),$$
$$a_{33} = -\left(\frac{1}{2}\right)h_z - 1 - \left(\frac{2}{3}\right)(\alpha - f),$$
$$a_{44} = +\left(\frac{1}{2}\right)h_z - 1 - \left(\frac{2}{3}\right)(\alpha - f),$$
$$a_{55} = +\left(\frac{3}{2}\right)h_z + 1 + (\alpha - f),$$
$$a_{66} = +\left(\frac{5}{2}\right)h_z + 5 - \left(\frac{1}{3}\right)(\alpha - f),$$
$$a_{21} = a_{12} = a_{65} = a_{56} = \left(\frac{\sqrt{5}}{2}\right)h_x,$$
$$a_{32} = a_{23} = a_{54} = a_{45} = \sqrt{2}\,h_x,$$
$$a_{43} = a_{34} = \left(\frac{3}{2}\right)h_x,$$
$$-a_{41} = a_{14} = a_{63} = -a_{36} = i\left(\frac{2\sqrt{5}}{3}\right)\alpha,$$
$$h_i = g\beta H_i/D\ (i = x, z), \quad \alpha = a/D, \quad f = F/D.$$

The eigenvalues of (10) ϵ_i are related to the eigenvalues of the Hamiltonian in (9) E_i by (5).

From the point of view of computing energy levels and probabilities, the simplest case is the one in which the external magnetic field is parallel or perpendicular to the trigonal axis of the crystalline field (optical axis of the crystal).

The expressions for the energy levels in these cases can be given in analytical form.[27,28] The corresponding curves for the energy levels are given in Figs. 4 and 5.

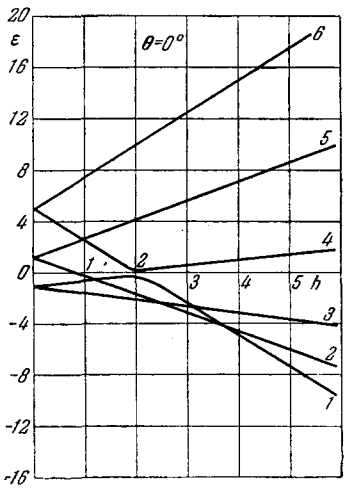

FIG. 4. Energy levels of the Fe^{3+} ion in corundum ($\theta = 0°$).

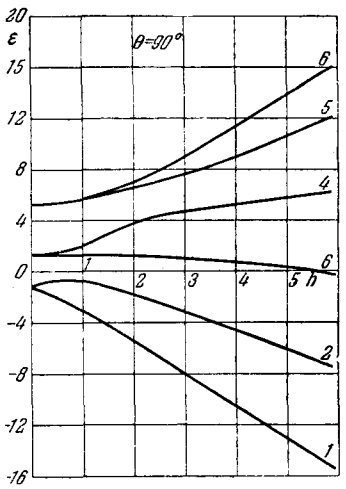

FIG. 5. Energy levels of the Fe^{3+} ion in corundum ($\theta = 90°$).

A promising material for paramagnetic amplifiers is rutile (crystalline titanium dioxide TiO_2) doped with the paramagnetic ions Cr^{3+} or Fe^{3+}, which isomorphically replace some of the Ti^{4+} ions. The crystallography of rutile has been studied in detail in [29].

The six O^{2-} ions surrounding each cation form a crystalline field of rhombic symmetry. The rutile crystalline lattice exhibits two kinds of nonequivalent cations, which are distinguished by the position of the neighboring oxygen ions; one type is converted into the other by rotation of the lattice through 90° about the tetragonal axis, which is usually called the c axis.

The energy levels of the two nonequivalent ion systems coincide at certain orientations of the crystal with respect to the external magnetic field. This situation arises when the magnetic field is parallel to the c axis and represents the case of greatest interest for practical purposes.

To analyze the EPR spectra of the Cr^{3+} and Fe^{3+} ions in rutile it is convenient to introduce a coordinate system in which the x, y, and z axes are in the $(\bar{1}10)$, (001), and (110) directions for one system of nonequivalent ions and in the $(\bar{1}\bar{1}0)$, (001), and $(\bar{1}10)$ directions for the other. The x and z axes for the second system are obtained by rotation of the corresponding axes of the first system through 90° about the y axis, which is in the same direction for both systems, and coincides with the c axis.

The spin Hamiltonian for the Cr^{3+} ion is written in the form

$$\hat{\mathcal{H}} = g\beta\mathbf{H}\hat{\mathbf{S}} + D\left[\hat{S}_z^2 - \frac{1}{3}S(S+1)\right] + E(\hat{S}_x^2 - \hat{S}_y^2) \quad (S = {}^3/_2) \tag{11}$$

with the following values of the constants:[30]

$$g = 1.97 \pm 0.01,$$
$$D = (-0.68 \pm 0.005)\ \text{cm}^{-1},$$
$$E = (-0.14 \pm 0.005)\ \text{cm}^{-1}.$$

The energy level diagram for the case in which the external field is parallel to the c axis is shown in Fig. 6.

The behavior of the levels of the Fe^{3+} ion in rutile can be described by the spin Hamiltonian[31]

$$\hat{\mathcal{H}} = g\beta\mathbf{H}\hat{\mathbf{S}} + D\left(\hat{S}_z^2 - \frac{35}{12}\right) + E(\hat{S}_x^2 - \hat{S}_y^2) + \frac{a}{6}\left(\hat{S}_x^4 + \hat{S}_y^4 + \hat{S}_z^4 - \frac{707}{16}\right) + \frac{7}{36}F\left(\hat{S}_z^4 + \frac{95}{14}\hat{S}_z^2 + \frac{81}{16}\right), \tag{12}$$

with the constants

$$g = 2.000 \pm 0.005,$$
$$D = (0.678_3 \pm 0.003_3)\ \text{cm}^{-1},$$
$$E = (0.073_6 \pm 0.002_3)\ \text{cm}^{-1},$$
$$a = (0.036 \pm 0.007)\ \text{cm}^{-1},$$
$$F = (-0.017 \pm 0.010)\ \text{cm}^{-1}.$$

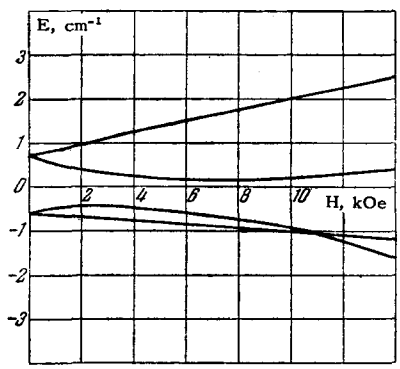

FIG. 6. Energy levels of the Cr^{3+} ion in rutile. Magnetic field parallel to the c axis.

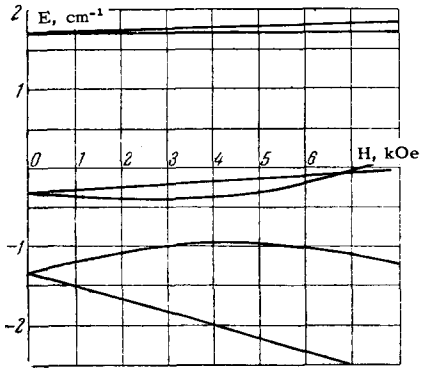

FIG. 7. Energy levels of the Fe^{3+} ion in rutile (H parallel to c axis).

In Fig. 7 we show the energy levels for this ion again with the external magnetic field parallel to the c axis.

The application of the above-mentioned crystalline compounds in quantum-mechanical amplifiers will be discussed below.

We now consider several typical optical spectra of paramagnetic crystals. Chromium corundum (ruby), whose lower energy levels have been considered in detail above, finds wide application in quantum-mechanical devices for the optical region. As we have already indicated, the ground term of the free chromium ion is ^4F. The ^2G term lies above it. The terms are split by the interaction with the crystalline field. A diagram showing the behavior of the energy levels of the chromium ion with the gradual application of crystalline fields of cubic and trigonal symmetry, taking account of the spin-orbit coupling, is shown in Fig. 8. An experimental investigation of the ruby optical absorption spectrum shows that there are two wide bands, the U band (approximately 18,000 cm^{-1}) and the Y band (approximately 25,000 cm^{-1}), and several groups of narrow lines, corresponding to transitions with energies of approximately 14,400 and and 21,000 cm^{-1}. [16]

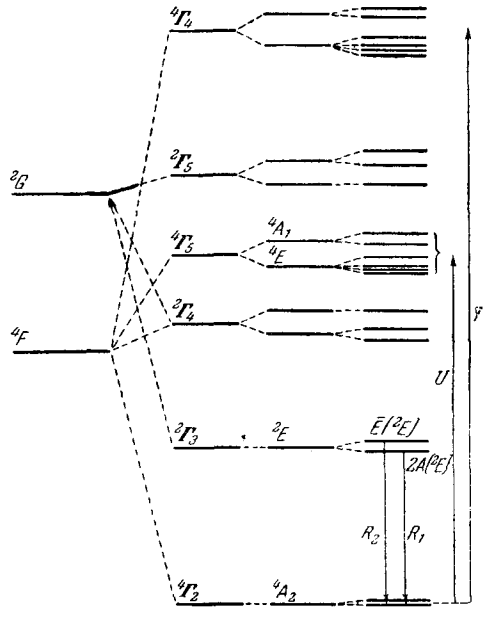

FIG. 8. Diagram showing the optical transitions of the Cr^{3+} ion in corundum.

The two narrow red lines R_1 —14,418 cm^{-1} and R_2 —14,447 cm^{-1} are especially characteristic of ruby. Both are fluorescence lines.

The wide absorption bands are due to transitions from the ground state $^4A_2$ to various components of the $^4\Gamma_5$ and $^4\Gamma_4$ levels. These levels have the same spin multiplicity.

The narrow lines correspond to transitions between the ground state $^4A_2$ and the $\bar{E}(^2E)$ level (the R_1 line) and the $\overline{2A}(^2E)$ level (R_2 line). The widths of the R_1 and R_2 lines depend on the chromium concentration in the corundum and on the temperature; at a concentration of 0.05% the width of the R_1 line is 0.32 cm^{-1} at 77°K and 0.25 cm^{-1} at 4.2°K. [32]

The two blue lines correspond to transitions between the $^4A_2$ level and components of the $^2\Gamma_5$ level.

Fluorescence of the red lines in ruby is observed in excitation in the wide absorption bands. The lifetime of the excited state ^2E is 5×10^{-3} sec as measured at 77°K.

As another example we consider the crystal fluorite doped with ytterbium. The Yb^{3+} ion is the simplest representative of the rare-earth group of the transition elements. It has 13 electrons, that is to say, it lacks one electron toward a completely filled shell. The paramagnetic and optical spectra of Yb^{3+} in CaF_2 have been investigated recently. [39] The Yb^{3+} ion replaces the Ca^{2+} ion in the CaF_2 lattice. The surrounding F^- ions create a crystalline field of cubic symmetry at the site of the paramagnetic ion. The ground term of the Yb^{3+} ion is $^2F_{7/2}$. The next term $^2F_{5/2}$ is located approximately 10,300 cm^{-1} higher.

The degeneracy of the levels with respect to the projection of J is partially lifted in the crystalline field. The lower term splits into two Kramers doublets (Γ_7 and Γ_6) and a quadruplet (Γ_8) while the upper term splits into a doublet (Γ_7) and a quadruplet (Γ_8) (Fig. 9).

The level degeneracy is totally removed when the external magnetic field is applied. The lower Kramers doublet has an isotropic g factor of $^{24}/_7$. The optical spectrum of the CaF_2 crystal with Yb^{3+} consists of several lines and a band in the visible and ultraviolet, corresponding to transitions between configurations. The lines are observed at 10,231, 10,235, and 10, 243 cm^{-1} in the infrared region, corresponding to transitions between components of the $^2F_{7/2}$ and $^2F_{5/2}$ terms; there are also weak bands at 11,013 and 8,084 cm^{-1}. The total splitting of the lower term (spacing between the $^2\Gamma_6$ and $^2\Gamma_7$ levels) is approximately 12 cm^{-1}. This material may be suitable for paramagnetic amplifiers in the submillimeter region. [33]

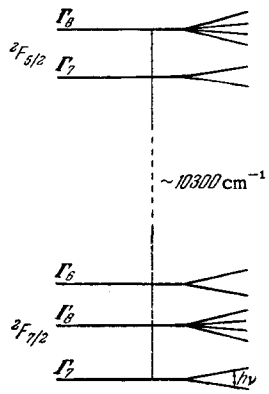

FIG. 9. Energy levels of the Yb^{3+} ion in CaF_2.

III. RELAXATION EFFECTS IN PARAMAGNETIC CRYSTALS

The possibility of obtaining negative temperatures in the energy level system of a paramagnetic ion in a crystal and thus, the possibility of using the crystal for generation or amplification of electromagnetic waves, depends strongly on relaxation processes in the crystal. These processes include spin-lattice and spin-spin interactions. In paramagnetic maser amplifiers these relaxation processes determine such important characteristics as gain, bandwidth, maximum signal amplitude (determined by saturation), and the time required for restoring amplification after a strong signal is removed. In maser oscillators the relaxation processes determine the amplitude of the oscillations that are generated. In addition, relaxation effects determine the amount of auxiliary or pump radiation required for inverting the populations of the energy levels.

The interaction of a paramagnetic crystal with an electromagnetic radiation field can be represented by the diagram shown in Fig. 10. The paramagnetic crystal can be regarded as consisting of a system of electron spins (spin system) and the lattice. It is assumed in this analysis that to a first approximation the spin system is free and weakly coupled to the lattice. Under these conditions equilibrium within the spin system is established much more rapidly than the equilibrium between the spin system and the lattice. The external electromagnetic radiation induces resonance magnetic dipole transitions between the energy levels. The population distribution in the levels of the spin system, which is in thermal equilibrium with the lattice, is governed by the Boltzmann relation.

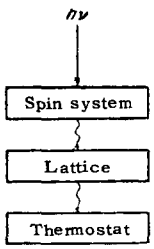

FIG. 10. Diagram showing the relaxation scheme in a paramagnetic crystal.

The probability of induced transitions is the same for transitions from a lower level to an upper level or vice versa; hence, when the spin system is in thermal equilibrium it absorbs energy from the external radiation and, by virtue of the spin-lattice interaction, transfers it to the lattice; in turn, the lattice transfers the energy to the thermostat. The spin-lattice interaction provides a mechanism for continuous absorption of the external radiation energy by the spin system, which maintains a constant Boltzmann distribution of paramagnetic ions over the energy levels. At high temperatures the rate of transfer of energy from the spin system to the thermostat is usually limited by the spin-lattice interaction. In this case the lattice itself serves as the thermostat for the spin system. At very low temperatures, however, (liquid helium temperatures or lower) the lattice may not act as a thermostat for the spin system and the "bottleneck" in the relaxation process is then the interaction of the lattice with the thermostat. Effects of interest in this connection have been discussed by several authors. [45, 64, 67, 72, 134] The experiments that have been carried out show that these effects are not of importance for the crystals and temperatures used in maser amplifiers.

a) Spin-lattice relaxation. The interaction of a spin system with a lattice can be realized by various mechanisms. The basic theory of spin-lattice relaxation has been given in [34-36] and has been developed in detail for various paramagnetic ions in [37-43]. The primary spin-lattice interaction mechanism in crystals is usually the Kronig-Van Vleck mechanism, in which the interaction between the spin system and the lattice takes place as follows: the thermal vibrations of the lattice modulate the electric crystalline field which, in turn, induces transitions in the spin system through the agency of spin-orbit coupling. In another mechanism, the Waller effect, the spin system exchanges energy with the thermal vibrations of the lattice via modulation of the magnetic interactions between the paramagnetic ions; this modulation is due to thermal vibrations. This mechanism can be of importance for ions in s states,[37] in which case the orbital moment is identically zero and the interaction of the spins with the electric crystalline field can occur only by virtue of mixing of the higher orbital states.

The strength of the spin-lattice interaction is usually characterized by a spin-lattice relaxation time, which is defined in terms of the probability of relaxation transitions between levels of the spin system induced by phonons in the lattice. The exchange of energy between lattice phonons and the spin system occurs via single-phonon and double-phonon processes. In the single-phonon process there is a resonance exchange of energy between the spin system and the lattice. In this case the phonon frequencies coincide with the frequencies of transitions between levels in the spin system. The double-phonon energy exchange be-

tween the spin system and the lattice takes place through combination scattering of phonons. Two phonons participate in this process and the difference in phonon frequencies is equal to the frequency of the transition between spin levels. Single-phonon processes usually occur in spin-lattice relaxation at liquid helium temperatures. In these processes the dependence of the spin-lattice relaxation time T_1 on temperature is given by $T_1 \sim T^{-1}$ when the spacing between levels is smaller than kT. If the level splitting is greater than kT there can be deviations from this relation.[70] At high temperatures spin-lattice interactions usually occur primarily through combination processes. These are characterized by a more rapid dependence of the spin-lattice relaxation time on temperature. When the spin-lattice relaxation takes place via the Kronig-Van Vleck mechanism the relaxation time depends to a large extent on Δ, the splitting of the orbital levels in the crystalline electric field, and the spin-orbit coupling constant λ. For the simple case of an ion with spin $S = \frac{1}{2}$ the spin-lattice relaxation time can be described by the formulas:[35, 36]

for single-phonon processes:

$$T_1 = C_1 \frac{\Delta^4}{\lambda^2 T}, \tag{13}$$

for combination scattering processes:

$$T_1 = C_2 \frac{\Delta^6}{\lambda^2 T^7}, \tag{14}$$

if T is smaller than the characteristic Debye temperature θ and

$$T_1 = C_2 \frac{\Delta^6}{\lambda^2 T^2},$$

if $T > \theta$. Here, the coefficients C_1 and C_2 contain the dependence on magnetic field and crystal parameters (density, velocity of sound etc.). The formulas become more complicated when $S = \frac{3}{2}$ but the dependence on temperature and on the constants Δ and λ remains the same as in the $S = \frac{1}{2}$ case.[36] We shall not discuss further the various theoretical aspects of spin-lattice relaxation, but refer the reader to a monograph on paramagnetic resonance[12] and to[44], where these questions are considered in detail.

b) Spin-spin relaxation. The establishment of equilibrium within the spin system plays an important role in the relaxation process. As we have noted above, in the analysis of the relaxation scheme in a paramagnetic crystal it is usually assumed that equilibrium is established within the spin system much more rapidly than between the spin system, considered as a whole, and the lattice vibrations. Hence, relaxation within the spin system and relaxation between the spin and the lattice can be characterized by two different times: T_2 is the spin-spin relaxation time and T_1 is the spin-lattice relaxation time, where $T_2 \ll T_1$. In many cases, however, the description of the relaxation process in terms of two relaxation times is not an accurate one. This situation arises in systems containing many energy levels, which are frequently used in maser amplifiers and oscillators; it is then important, as we shall see below, to know the probability of spin-lattice transitions between individual energy levels and to know the rate at which equilibrium is established within the spin level system itself. As pointed out in[45], a very important effect in the establishment of equilibrium within the spin system is the cross-relaxation process, in which energy is transferred between different levels of the spin system. The cross-relaxation process is especially pronounced in paramagnetic maser amplifiers and oscillators used in the microwave region. If the level spacing is uniform a Boltzmann population distribution over different spin energy levels is established in a time of order T_2. When the level splitting is not uniform equilibrium with the lattice is reached in a time T_1. However, when the splittings for different level pairs are approximately the same or approximately multiples of each other, equilibrium between these levels can be established in the spin-spin cross relaxation time T_{12}, which is much shorter than T_1. The cross-relaxation time T_{12} can be determined in terms of the probability of a transition of one ion due to the effect of an inverse transition in one or more neighboring ions. Two Gaussian lines have a cross relaxation transition probability given by[45]

$$w_{ij} = (2\pi)^{-1/2} \hbar^{-2} |\mathcal{H}_{ij}|^2 [(\Delta\nu_\alpha)^2 + (\Delta\nu_\beta)^2]^{-2} \times \exp\left\{ -\frac{(\nu_\alpha - \nu_\beta)^2}{2[(\Delta\nu_\alpha)^2 + (\Delta\nu_\beta)^2]} \right\}, \tag{15}$$

where $(\Delta\nu_\alpha)^2$ and $(\Delta\nu_\beta)^2$ are the second moments of the absorption lines. This formula is obviously approximate. The higher moments must be used to determine w_{ij} with higher accuracy. It follows from (15) that the probability of cross-relaxation transitions is determined essentially by the degree of overlap of the α and β transitions (overlap of the functions $g_\alpha(\nu)$ and $g_\beta(\nu)$). The overlap function has been calculated in[46] by the moment method and the results have been used to determine the dependence of this quantity on the magnetic dilution of the interacting paramagnetic ions.

In Fig. 11 we show two typical spin systems in which cross relaxation can be of importance. These

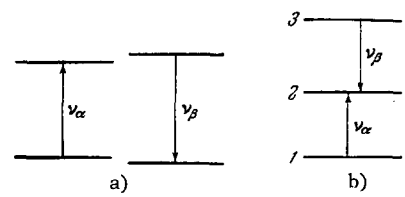

FIG. 11. Examples of cross-relaxation transitions in a system comprising two pairs of energy levels with approximately the same splitting.

are systems with two transitions at approximately the same frequency: a) α and b) β.

Cross relaxation is also important in systems in which the transition frequencies are multiples of each other. This case is frequently encountered in paramagnetic crystals. Cross relaxation between level spacings that are multiples of each other is characteristic of the reorientation of three or more spins. Figure 12 illustrates multiple cross-relaxation transitions of this kind. In this figure we show a system consisting of four energy levels E_1, E_2, E_3, and E_4 with $E_2 - E_1 \approx 2(E_4 - E_3)$.

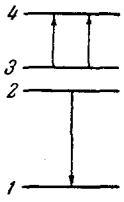

FIG. 12. Cross-relaxation transitions in a level system in which one splitting is twice another.

Cross relaxation in this system operates in the following way: radiation of a photon $h\nu_{21}$ by one ion is accompanied by simultaneous absorption of two photons $h\nu_{43}$ by two ions. This kind of multiple transition has been observed experimentally in [47-49] and plays a very important role in quantum-mechanical amplifiers. As in the case of cross relaxation between level pairs with approximately the same spacing, cross-relaxation transitions for frequencies related by integral ratios will occur even with inexact coincidence (several hundreds of megacycles with the line widths of the individual resonance transitions being several tens of megacycles).[50,51]

1. Physical fundamentals of microwave maser amplifiers. Consider the change in population of spin levels of a paramagnetic ion in a crystal under the influence of an external electromagnetic field and thermal vibrations of the lattice. For simplicity we first consider a system of spins with two energy levels, E_1 and E_2. The change in the populations n_1 and n_2 with time is described by the kinetic equation

$$\frac{dn_1}{dt} = -n_1 w_{12} + n_2 w_{21} + (n_2 - n_1) W_{12} \qquad (16)$$

with the requirement that the number of particles be conserved

$$n_1 + n_2 = N.$$

Here w_{12} and w_{21} are the transition probabilities due to the spin-lattice interaction; these are related by the expression $w_{12} = w_{21} \exp\left(-\frac{E_2 - E_1}{kT}\right)$* while W_{12} is the probability for induced transitions under the effect of the microwave field at the resonance frequency $\nu = (E_2 - E_1)/h$.

*This relation follows directly from the condition that at thermal equilibrium the populations must obey a Boltzmann distribution.

If the equilibrium Boltzmann distribution is disturbed these equations describe the rate at which equilibrium is restored. If the population difference is $\Delta n_{12} = n_1 - n_2$ the solution is given by

$$\Delta n_{12}(t) - \Delta n_{12}^0 = [\Delta n_{12(t=0)} - \Delta n_{12}^0] \exp\left(-\frac{t}{T_1'}\right), \qquad (17)$$

where Δn_{12}^0 is the equilibrium population difference, $\Delta n_{12(t=0)}$ is the difference in populations determined by the initial conditions at $t = 0$, and the time

$$T_1' = \frac{1}{w_{12} + w_{21} + 2W_{12}} \qquad (18)$$

with $W_{12} = 0$ is the spin-lattice relaxation time. If $W_{12} \neq 0$ the spin system reaches equilibrium more rapidly but the stationary state that is achieved does not correspond to a Boltzmann distribution. In this case the stationary population difference is

$$(\Delta n_{12})_{stat} = \frac{\Delta n_{12}^0}{1 + 2T_1 W_{12}}. \qquad (19)$$

It then follows that saturation effects can arise if the probability of induced transitions is comparable with the probability of spin-lattice transitions $W_{12} \sim w_{12}$, w_{21}. The difference in level populations approaches zero as $W_{12} \to \infty$. The probability of induced transitions is given by (7). For the case of magnetic dipole transitions and a Lorentz line shape

$$W_{12} = \frac{1}{4}\gamma^2 H_1^2 |\langle S_x \rangle_{12}|^2 2T_2, \qquad (20)$$

where $\gamma = 2\pi g\beta/h$, H_1 is the intensity of the microwave magnetic field that induces the transitions, $\langle S_x \rangle_{12}$ is the matrix element of the electron spin operator, and T_2 is the spin-spin relaxation time. In this case (19) is rewritten in the form

$$(\Delta n_{12})_{stat} = \frac{\Delta n_{12}^0}{1 + \gamma^2 H_1^2 |\langle S_x \rangle_{12}|^2 T_1 T_2}. \qquad (19a)$$

The quantity $S = \gamma^2 H_1^2 |\langle S_x \rangle_{12}|^2 T_1 T_2$ is called the saturation factor.

Consider a three-level system (Fig. 13) with saturation between levels 1 and 3 produced by radiation at frequency ν_{31}; in this system it is possible to have a surplus population in level 3 as compared with level 2 (or level 2 compared with level 1).[52,53] This situation corresponds to a negative spin temperature between levels 3 and 2 (2 and 1). Under these conditions the system becomes active, that is to say, it is capable of radiating energy at a frequency ν_{32} (or ν_{21}).

Weak radiation applied between levels 2 and 3 will be amplified as a consequence of induced transitions. A maser amplifier of this kind can operate as an oscillator if the induced radiation is large enough to compensate for the losses in the microwave system in which the paramagnetic crystal is located. Let us

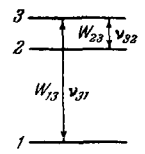

FIG. 13. Diagram of a three-level system.

consider the requirements for obtaining negative temperatures in a three-level system. We shall treat the problem assuming that there is no cross relaxation. The equations describing the level populations are:[53]

$$\left.\begin{aligned}\frac{dn_1}{dt} &= -(w_{12}+w_{13})n_1 + w_{21}n_2 + w_{31}n_3 - (n_1-n_3)W_{13},\\ \frac{dn_2}{dt} &= -(w_{21}+w_{23})n_2 + w_{12}n_1 + w_{32}n_3 - (n_2-n_3)W_{23},\\ n_1+n_2+n_3 &= N,\end{aligned}\right\} \quad (21)$$

where N is the total population in the levels and

$$w_{12} = w_{21}\exp\left(-\frac{h\nu_{21}}{kT}\right),$$

$$w_{13} = w_{31}\exp\left(-\frac{h\nu_{31}}{kT}\right),$$

$$w_{23} = w_{32}\exp\left(-\frac{h\nu_{32}}{kT}\right)$$

are the probabilities for relaxation transitions between corresponding levels under the effect of the thermal vibrations of the lattice. Under stationary conditions ($dn_1/dt = dn_2/dt = dn_3/dt = 0$), if the pump power is high ($W_{13} \gg W_{23}$, w_{ik}; $k = 1, 2, 3$) we have

$$n_1 - n_2 = n_3 - n_2 = N\frac{(w_{21}-w_{12})-(w_{32}-w_{23})}{(2w_{21}+w_{12})+(w_{32}+2w_{23})+3W_{23}}. \quad (22)$$

When $h\nu_{31} \ll kT$ we have

$$n_1 - n_2 = n_3 - n_2 = \frac{1}{3}\frac{hN}{kT}\frac{w_{21}\nu_{21}-w_{32}\nu_{32}}{w_{21}+w_{32}+W_{23}}. \quad (22a)$$

It is evident from this formula that if a population inversion is to be produced in levels 3 and 2 (as compared with the equilibrium distribution) we must satisfy the condition $w_{21}\nu_{21} > w_{32}\nu_{32}$. This condition corresponds to a negative temperature at frequency ν_{32}. If the inverse inequality holds $w_{21}\nu_{21} < w_{32}\nu_{32}$ we have negative absorption at the frequency ν_{21}. The population inversion can be characterized by the quantity

$$I_{32} = \frac{n_3-n_2}{(n_3-n_2)_0}, \quad (23)$$

where $(n_3-n_2)_0$ is the equilibrium population difference in the absence of pump radiation. We shall call the quantity I_{32} the inversion coefficient. The power radiated at frequency ν_{32} is given by

$$P_{mag} = \frac{N}{3kT}(h\nu_{32})^2 I_{32}W_{32}. \quad (24)$$

The negative absorption can be related to a negative Q

$$|Q_m| = \frac{2\pi\nu P}{P_{mag}}, \quad (24a)$$

where P is the energy of the electromagnetic field in the crystal. It is evident from (22a) that the higher the frequency of the pump power ν_{31} and the probability of the relaxation transition w_{21}, the easier it is to obtain a negative temperature between levels 3 and 2.

The conditions that must be satisfied to obtain negative temperatures in a four-level system are derived in the same way as for a three-level system and can be obtained easily by solving kinetic equations similar to those in (21). In a four-level system, however, it is possible to use pump radiation between two pairs of levels. The application of pump radiation between two pairs of levels can increase the inversion I. The pump power can be applied in various ways in a four-level system; three examples are shown in Fig. 14. In the scheme shown in Fig. 14a pump radiation is applied at two frequencies ν_{p1} and ν_{p2}. Under these conditions the population difference between levels 3 and 4 is given by:[54]

$$(n_4-n_3)_1 = \frac{Nh}{4kT}\frac{w_{32}\nu_{32}+w_{31}\nu_{31}-w_{43}\nu_{43}}{w_{34}+w_{23}+w_{13}+W_{43}}. \quad (25)$$

If the pump radiation is applied to only one pair of levels, for example $2 \longleftrightarrow 4$, we have

$$(n_4-n_3)_2 = \frac{Nh}{4kT}\frac{w_{31}(w_{21}\nu_{32}-\nu_{41}w_{43})+(w_{41}+w_{31}+w_{21})(w_{32}\nu_{32}-w_{43}\nu_{43})}{w_{31}(w_{41}+w_{21})+(w_{41}+w_{31}+w_{21})(w_{43}+w_{32}+W_{43})}; \quad (26)$$

comparison of (25) and (26) shows that a higher inversion coefficient can be achieved by pumping at two frequencies.

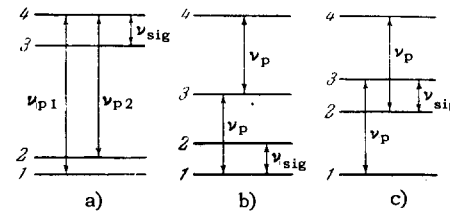

FIG. 14. Four-level systems

In the scheme shown in Fig. 14b the pump power is applied between two transitions $1 \longleftrightarrow 3$ and $3 \longleftrightarrow 4$ with the same transition frequency. In this case the inversion coefficient for the $2 \longleftrightarrow 1$ transition is given by:[55]

$$(I_{21})_1 = \frac{\nu_{32}}{\nu_{21}}\left[\frac{w_{32}+2w_{24}+\frac{\nu_{21}}{\nu_{32}}(w_{42}-w_{21})}{w_{21}+w_{32}+w_{42}}\right] \quad (27)$$

However, if the $3 \longleftrightarrow 4$ transition is not saturated then

$$(I_{21})_2 = \frac{w_{42}(w_{43}\nu_{43}+w_{41}\nu_{41}+w_{32}\nu_{32})-(w_{43}+w_{41})(w_{21}\nu_{21}+w_{42}\nu_{42}-w_{32}\nu_{32})}{\nu_{21}[(w_{32}+w_{21})(w_{43}+w_{41})+w_{42}(w_{32}+w_{21}+w_{41}+w_{43})]}. \quad (28)$$

If all the relaxation probabilities are the same in (27) and (28) then

$$(I_{21})_1 \approx 4(I_{21})_2,$$

that is to say, the application of pump power at two transitions provides a considerable increase in the inversion coefficient.

The spacing between levels 1 and 3 and 2 and 4 is the same in the level system shown in Fig. 14c. Hence pump power at the same frequency $\nu_p = \nu_{31} = \nu_{42}$ causes enrichment of level 3 and depletion of level 2

simultaneously. As a result of this symmetric effect (due to the pump radiation) the difference in the populations in levels 3 and 2 becomes [56]

$$n_3 - n_2 = \frac{Nh}{4kT} \frac{w_{41}\nu_{41} + w_{43}\nu_{43} + w_{21}\nu_{21} - w_{32}\nu_{32}}{w_{12} + w_{23} + w_{14} + w_{34}} \quad (29)$$

If the pump power is applied only between two levels, for example 1 and 3, then

$$(n_3 - n_2)_1 = \frac{Nh}{4kT} \frac{w_{42}(w_{41}\nu_{21} - w_{43}\nu_{32}) + (w_{41} + w_{42} + w_{43})(w_{21}\nu_{21} - w_{32}\nu_{32})}{w_{42}(w_{41} + w_{43}) + (w_{41} + w_{42} + w_{43})(w_{21} + w_{32})}. \quad (29a)$$

A comparison of (29) and (29a) shows that the symmetric version yields an appreciable increase in the inversion coefficient for the $3 \longleftrightarrow 2$ transition. In particular, if the probabilities for relaxation transitions are the same between all levels we have

$$\frac{I_{\text{symm}}}{I_1} = \frac{n_3 - n_2}{(n_3 - n_2)_1} = \frac{1}{2}\left(\frac{\nu_{41} + \nu_{43}}{\nu_{21} - \nu_{32}} + 1\right). \quad (29b)$$

We now consider the effect of cross relaxation on the operation of maser amplifiers. As already noted, cross-relaxation transitions cause a change in the level populations and can thus have an important effect on the operation of maser amplifiers. Cross relaxation is important because it can reduce the time needed to establish equilibrium between various energy levels of a paramagnetic ion in a crystal, thereby modifying the conditions required for obtaining negative temperatures between the levels. For example, if cross relaxation accelerates the establishment of equilibrium between levels 3 and 2 (cf. Fig. 13), it then follows from (22a) that the effect will be to worsen the condition for obtaining a negative temperature between these levels. On the other hand, if cross relaxation shortens the relaxation time for the $1 \longleftrightarrow 2$ transition, it increases the positive difference in populations between levels 3 and 2. A cross-relaxation effect of this kind has in fact been observed in paramagnetic maser amplifiers. [50,57,58] In corundum, rutile, and other crystals with Cr^{3+} as the impurity there are four energy levels and cross relaxation is found to be important between level pairs with splittings that are integral ratios. The probability of these transitions increases with increasing Cr^{3+} concentration. Cross-relaxation transitions are especially important at helium temperatures because the spin-lattice relaxation time becomes longer as the temperature is reduced whereas the probabilities of cross relaxation transitions remain essentially unchanged down to the very lowest temperatures. Because of cross-relaxation effects, paramagnetic ruby amplifiers with Cr^{3+} concentrations greater than 0.05% do not work at helium temperatures whereas they do operate with higher concentrations at higher temperatures. [57]

An analysis of the effect of cross relaxation on the characteristics of paramagnetic amplifiers has been given in [51]. It should be noted that the quantitative estimates in [51] are based on the assumption that the probabilities for spin-lattice transitions are proportional to the probabilities for magnetic dipole transitions, although this can hardly be the case.

It is of interest to investigate the possibility of using crystals with two impurity ions as a means of improving the characteristics of paramagnetic amplifiers. The energy levels of one of these ions are used for amplification; the levels of the second ion are chosen to increase the probability of relaxation transitions between appropriate levels of the first ion. The second ion must have a shorter spin-lattice relaxation time. Thus, in the paramagnetic amplifier using gadolinium ethyl sulfate [59] the second impurity in the crystal was obtained by adding Ce^{3+}, whose spin-lattice relaxation time is shorter than that of Gd^{3+}. Amplification was achieved in this crystal although it could not be achieved without the cerium impurity.

2. Experimental techniques for investigating relaxation processes. Relaxation processes in paramagnetic crystals are investigated through the effect of saturation. Continuous or pulsed saturation of the paramagnetic resonance lines can be employed.

According to (19) above, under stationary conditions of continuous saturation the intensity of the line associated with the transition between levels i and j is given by

$$J = J_0 \frac{1}{1 + \gamma^2 H_1^2 |\langle S_x \rangle_{ij}|^2 T_1 T_2}, \quad (30)$$

where J_0 is the line intensity in the absence of saturation.

The spin-lattice relaxation time T_1 can be determined by measuring the ratio J/J_0 provided the quantities γ, $\langle S_x \rangle_{ij}$, and T_2, which characterize the line and the intensity of the saturating microwave magnetic field in the resonator in which the sample is located, are known. The quantity H_1 can be computed from the resonator Q and the applied power. Thus, for a rectangular cavity excited in the TE_{102} mode the maximum field strength at the end wall is

$$H_1^2 = \frac{16PQ}{\nu V \left(\frac{\lambda_g}{\lambda}\right)^2}, \quad (31)$$

where P is the power of the microwave field in the cavity (erg/sec), ν is the frequency (cps), V is the cavity volume (cm^3), λ and λ_g are respectively the wavelength in free space and in a waveguide with the same cross-section dimensions as the cavity. The spin-spin relaxation time T_2 can be determined from the observed line width. For a Lorentz line we have

$$T_2 = \frac{1}{\pi \Delta\nu}, \quad (32)$$

where $\Delta\nu$ is the line width at half intensity. The time T_1 calculated in this way is the spin-lattice relaxation time if there are no cross relaxation effects. However, if these effects are of importance the time T_1 determined by the continuous saturation technique (30) will represent an effective relaxation time characterizing

the spin-lattice and spin-spin cross-relaxation interactions. For this reason the continuous saturation technique does not permit a detailed investigation of relaxation processes in multi-level systems.

There is a direct method for measuring the relaxation time, in which the spin-lattice and cross-relaxation interactions can be separated. This is the pulsed saturation technique. In this method the relaxation time is determined directly from the relaxation curve showing the restoration of line intensity after the saturation pulse is removed. [48,49,56,58,60-63,66,69,73,77,79]

Spin-lattice and spin-spin cross relaxation effects can be separated by using saturation pulses of different length. [62,79] If the shape of the relaxation curve depends on the length of the saturating pulse this is an indication of the presence of cross-relaxation interactions in the transition being studied. If saturation takes place with short pulses whose lengths are less than the cross-relaxation times, these interactions will be clearly reflected in the relaxation curve.

To illustrate these effects, we show in Fig. 15 relaxation curves for a paramagnetic resonance line of Cr^{3+} in rutile [63] obtained with saturation pulses of different length.

The pulsed saturation technique can also be used to study transient processes in maser amplifiers if the saturation pulse is applied at the signal frequency or at the pump frequency. Two-frequency pulse saturation techniques can be used to determine the probabilities for relaxation transitions between different levels. [58]

3. Experimental data on relaxation in certain paramagnetic crystals. We now present a brief summary of relaxation processes in paramagnetic crystals presently used as working materials in maser amplifiers. In all cases we refer to corundum with Cr^{3+} and Fe^{3+}, potassium cobalticyanide with Cr^{3+}, rutile with Cr^{3+} and Fe^{3+} and lanthanum ethyl sulfate with Gd^{3+}.

1) Cr^{3+} in cyanide. The relaxation of Cr^{3+} in cyanide [K_3Cr, $Co(CN)_6$] has been studied in detail by various techniques. [50,58,64,66] The results can be summarized as follows. The spin-lattice relaxation time at helium temperatures is independent of the Cr^{3+} concentration in the range 0.03—1% and is reduced at concentrations higher than 1%. At these temperatures spin-lattice relaxation takes place via direct single-phonon processes and the relaxation time is given approximately by $T_1 \sim T^{-1}$.

The value of T_1 is somewhat different for different electronic transitions but the average value is approximately 3×10^{-2} sec at 1.4°K. Cross-relaxation effects are observed for two transitions at nearby frequencies. [50] The probability of cross-relaxation transitions is a strong function of the Cr^{3+} concentration and the spacing between transitions. The probabilities for spin-lattice transitions between individual Cr^{3+} levels in cyanide have been determined in [58].

2) Cr^{3+} and Fe^{3+} in corundum. Corundum with Cr^{3+} is one of the crystals used in microwave maser amplifiers. Relaxation effects in this material have been studied by many authors [48,49,56,68,69,80] over a wide range of temperatures and concentrations. The spin-lattice relaxation time is essentially independent of the Cr^{3+} concentration* in the range 0.002 + 0.1% at room temperature and varies slightly with different transitions, having an average value of approximately 3×10^{-6} sec.

The relaxation time becomes longer at liquid nitrogen and liquid helium temperatures; a noticeable reduction of the spin-lattice relaxation time is observed when the Cr^{3+} concentration is raised and this reduction is more pronounced at helium temperatures. At 77°K, T_1 varies between 1×10^{-4} and 4×10^{-6} sec for Cr^{3+} concentrations ranging from 0.015 to 0.65%. At this temperature T_1 varies somewhat for different transitions, with a typical value for a sample with a concentration of 0.05% being approximately 5×10^{-5} sec. A functional dependence of the form $T_1 \sim T^{-5}$—T^{-7} is observed at liquid nitrogen temperatures.

Cross relaxation plays an important role at liquid helium temperatures. Cross-relaxation interactions in the Cr^{3+} spectrum have been observed and investigated for various ratios of the splittings between energy levels.

In the analysis of relaxation by pulsed saturation techniques the relaxation curve is described by a sum of exponentials: there is a "fast" exponential, which characterizes the change in population difference due to cross-relaxation interactions, and a "slow" exponential, which characterizes the spin-lattice relaxation. To illustrate cross-relaxation effects, in Fig. 16 we show typical relaxation curves for the $\frac{1}{2} \longleftrightarrow -\frac{1}{2}$ transition obtained in a sample with a Cr^{3+} concentration of approximately 0.15% with the crystal oriented in various directions with respect to the external magnetic field. In the parallel orientation ($\theta = 0°$), the $\frac{1}{2} \longleftrightarrow -\frac{1}{2}$ transition is "shunted" by the $\frac{3}{2} \longleftrightarrow -\frac{3}{2}$ cross-relaxation transition whose frequency is exactly three times greater than that of the $\frac{1}{2} \longleftrightarrow -\frac{1}{2}$ transition. This effect is clearly evident on the relaxation

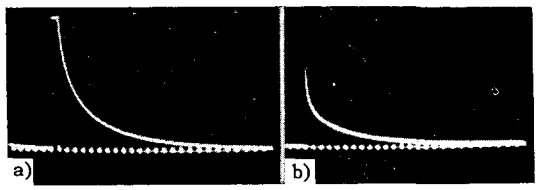

FIG. 15. Relaxation curves for one of the transitions in the Cr^{3+} spectrum in rutile obtained with two saturation pulses of different length: a) τ = 2 msec; b) τ = 0.05 msec. The time markers are spaced at 2 msec. T = 1.7°K.

*Here and in what follows the concentration of Cr^{3+} in Al_2O_3 is taken as the ratio of the number of Cr^{3+} ions to the number of Al^{3+} ions.

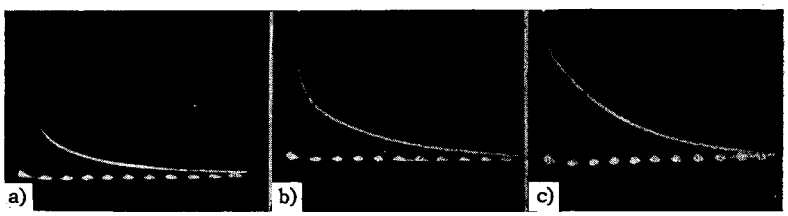

FIG. 16. Relaxation curves for the $1/2 \longleftrightarrow -1/2$ transition of Cr^{3+} in Al_2O_3 with different crystal orientations: a) $\theta = 0°$; b) $\theta = 10°$; c) $\theta = 15°$. The saturation pulse $\tau = 200$ msec. The time markers are spaced at 20 msec. $T = 4.2°K$.

curve for the $\frac{1}{2} \longleftrightarrow -\frac{1}{2}$ transition, which contains a fast cross-relaxation exponential. The weighting of the fast exponential is reduced appreciably as the crystal orientation is changed from the parallel direction, thereby disturbing the integral frequency ratio between the $\frac{1}{2} \longleftrightarrow -\frac{1}{2}$ and $\frac{3}{2} \longleftrightarrow -\frac{3}{2}$ transitions.

At helium temperatures spin-lattice relaxation in chromium corundum takes place via single-phonon processes and the spin-lattice relaxation time is given by $T_1 \sim T^{-1}$ although deviations from this relation have been observed at high Cr^{3+} concentrations.

The value of T_1 depends on the Cr^{3+} concentration and varies considerably for different transitions. For instance, at 4.2°K and $\theta = 90°$ in a sample with a Cr^{3+} concentration of approximately 0.03%, T_1 varies between 20 and 60 msec for various transitions. At this same temperature but with $\theta = 0°$ the value of T_1 for the $\frac{1}{2} \longleftrightarrow -\frac{1}{2}$ transition varies between 100 and 1 msec as the Cr^{3+} concentration is increased from 0.05 to 0.65%.

We note that the line width for the paramagnetic resonance of Cr^{3+} in corundum cannot be explained entirely by magnetic dipole interactions.[71] It is possible that exchange interactions make an appreciable contribution to this line width. Exchange interactions in chromium corundum can also affect the spin-lattice relaxation.[80]

The relaxation of Fe^{3+} in Al_2O_3 has been studied in [26,27,73]. At helium temperatures the value of T_1 varies with different transitions and when $\theta = 90°$ in a sample with an Fe^{3+} concentration of approximately 0.03% it amounts to 1.5—2 msec at 4.2°K and 4—13 msec at 1.4°K.

At higher temperatures the spin-lattice relaxation time is approximately 0.8 msec at 10.1°K, 0.5—1 sec at 20.2°K, and less than 10 μsec at $T > 56°K$.

3) Cr^{3+} and Fe^{3+} in rutile. Monocrystalline rutile (TiO_2) with Cr^{3+} or Fe^{3+} as an impurity is a suitable material for maser amplifiers in the millimeter region because of the high zero-field splitting of the spin levels in the crystalline field.[30,31,74-76] The relaxation of Cr^{3+} in rutile has been studied by pulse saturation techniques in [63] and [73]. At helium temperatures the spin-lattice relaxation time for various transitions varies within the limits 2.1—4.5 msec with $\theta = 90°$ at a frequency of 34.6 kMc.[73] At 9.4 kMc the spin-lattice relaxation is characterized by two quantities, T_1 and T_1', for each transition.[63] The values of T_1 and T_1' lie in the range 2.2—4 msec and 0.5—1.1 msec respectively. At helium temperatures a function weaker than T^{-1} (in certain transitions) describes the dependence of the spin-lattice relaxation time on temperature; this is related to the large splitting of the spin levels of Cr^{3+} in rutile. At higher temperatures the spin-lattice relaxation time is approximately 2 msec at 10.1°K, 0.6 msec at 20.3°K, and less than 10 μsec at $T > 56°K$. The relaxation time of Fe^{3+} in rutile at 4.2°K remains very much the same in different transitions, amounting to approximately 2 msec. At 1.7°K the relaxation for the same transitions is characterized by two times T_1 and T_1' lying within the limits 3.5—6 msec and 0.6—2.5 msec respectively. In certain transitions a function more rapid than T^{-1} describes the dependence of relaxation time on temperature in the region 4.2—1.7°K; as in the case of Cr^{3+} in rutile, this effect is associated with the high zero-field splitting of the energy levels.[63] Cross relaxation is observed in both Cr^{3+} and Fe^{3+} in rutile at helium temperatures.

4) Gd^{3+} in ethyl sulfate. The relaxation time for Gd^{3+} in ethyl sulfate [$La_{0.995}Gd_{0.005}(C_2H_5SO_4)_3 \cdot 9H_2O$] at helium temperatures is found to be different for different transitions. Thus at 4.2°K with the crystal axis parallel to the magnetic field T_1 varies from 2.6 msec to 9.8 msec in various electronic transitions.[60,78] The discrepancy between the values of T_1 as measured by continuous and pulsed saturation techniques[60] is probably due to cross relaxation between the levels of the Gd^{3+} ion. In a sample of ethyl sulfate containing the ion Ce^{3+} (Ce:La = 1:500; Gd:La = 1:200) there is an appreciable reduction of the relaxation time for the $-\frac{1}{2} \longleftrightarrow \frac{1}{2}$ transition in Gd^{3+} when this transition coincides with a transition between the Ce^{3+} levels.[78] This effect, which we have mentioned above, is due to cross-relaxation between the energy levels in Gd^{3+} and Ce^{3+}.

4. Materials for microwave paramagnetic amplifiers. The paramagnetic crystals considered above are used in microwave maser amplifiers. The basic requirements for working materials in paramagnetic amplifiers in which pump radiation is used can be formulated as follows.

First, the paramagnetic ion in the crystal must have at least three levels. For this reason ions with effective spins $S = \frac{1}{2}$ (for example, Ti^{3+}, Co^{2+}, Cu^{2+} and many rare-earth ions) cannot be used. The zero field splittings of the spin levels (zero magnetic field) are usually chosen on the basis of the frequency region for which the amplifier is intended.

In general the paramagnetic ions that are used do not have nuclear magnetic moments; the presence of hyperfine structure reduces amplifier efficiency since the number of ions in a given energy level is reduced.

The paramagnetic crystal must have suitable spin-lattice relaxation times. If T_1 is too short it is necessary to use appreciable pumping power to achieve saturation. If the relaxation times are too long the maximum signal amplitude is limited to very small values and it is difficult to restore gain rapidly after cutoff due to strong-signal saturation. In the materials presently in use $T_1 \sim 10^{-2}$—10^{-4} sec.

The ratios of relaxation transitions to various levels must favor negative temperatures between the desired level pairs.

The width of the paramagnetic line of material must not be excessive; optimum widths lie in the range 10—100 Mc.

Cross relaxation and line broadening set an upper limit on the paramagnetic ion concentration. The maximum allowable concentration of paramagnetic ions is usually 0.05—1% depending on the particular crystal, the frequency range, and the temperature.

Crystals in which all the paramagnetic ions are magnetically equivalent and form a single system with common energy levels are most suitable for paramagnetic amplifiers.

The crystal must be chemically inert, stable, and have low dielectric losses. One of the best crystals is corundum (Al_2O_3).

IV. QUANTUM MECHANICAL (PARAMAGNETIC) MICROWAVE AMPLIFIERS (MASERS)

Of all the quantum-mechanical amplifiers that have been proposed the most promising for continuous amplification is the pumped three-level paramagnetic amplifier.[52,53] There are various possible designs for the microwave devices in which the radiation interacts with the active material. We shall consider two of the most popular. In one the active material interacts with radiation in the form of a standing wave; in the other the radiation appears in the form of a traveling wave. The first is the cavity resonator paramagnetic amplifier and the second is the traveling-wave paramagnetic amplifier.

1. Cavity paramagnetic amplifier (CPA). Suppose that the active paramagnetic material is located in a cavity resonator. The width of the spectral line of paramagnetic crystals used in cavity amplifiers is usually greater than the bandwidth of the cavity itself so that the bandwidth of the CPA is determined by the bandwidth of the cavity. Since the active material is essentially a medium with negative losses the cavity resonator becomes regenerative and its natural bandwidth is reduced.

The relation between the gain and bandwidth of a CPA can be established from an analysis of a reflection CPA. In this case the signal reflected from the cavity is amplified. In Fig. 17 we show the equivalent circuit for such an amplifier connected to a line having a characteristic impedance Z_0 through a transformer with a coupling coefficient n equal to ωM, where M is the mutual inductance. Suppose that the negative resistance introduced by the active material is R_m and that the resistance characterizing the natural loss of the cavity is R_0.

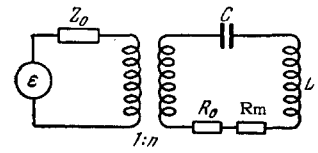

FIG. 17. Equivalent circuit of the CPA.

The reflection coefficient for the line loaded by the cavity amplifier is

$$\Gamma = \frac{\beta - 1}{\beta + 1} = K, \tag{33}$$

where $\beta = \dfrac{n^2/Z_0}{R_0 - |R_m|}$ and K is the voltage multiplication factor. Introducing $Q_0 = \dfrac{\omega L}{R_0}$, $Q_c = \dfrac{\omega L}{n^2/Z_0}$, and $Q_m = \omega L/R_m$ and assuming that the overall Q of the resonator is given by

$$Q^{-1} = Q_0^{-1} + Q_c^{-1} - |Q_m|^{-1}, \tag{34}$$

we have

$$\Gamma = \frac{2Q}{Q_c} - 1. \tag{35}$$

Replacing Γ by K, expressing Q_c in terms of Q_m and Q_0, and taking $Q = \nu/\Delta\nu$ we have

$$(K-1)\Delta\nu = 2\nu\left(\frac{1}{|Q_m|} - \frac{1}{Q_0}\right) = A, \tag{36}$$

where ν is the frequency of the amplified signal and $\Delta\nu$ is the amplifier bandwidth.

The quantity A is proportional to the signal frequency ν. Thus, for a given Q of the working material the bandwidth of an amplifier increases with frequency. When the line width is greater than the cavity bandwidth the product $(K-1)\Delta\nu$ is a constant for a given CPA and can be taken as a figure of merit. The value of A is independent of the coupling between the cavity and the line.

If the coupling is changed K and $\Delta\nu$ vary individually. Reducing the coupling causes K to increase but reduces $\Delta\nu$. Oscillation can occur if the coupling becomes small enough. This situation arises when

$$\frac{1}{Q_c^{cr}} = \frac{1}{|Q_m|} - \frac{1}{Q_0}, \tag{37}$$

i.e., $Q = \infty$. It is evident that the bandwidth of the CPA is a strong function of the gain.

Regeneration in the CPA leads to instability. If $Q_0 \gg |Q_m|$ then

$$K = \frac{|Q_m| + Q_c}{|Q_m| - Q_c}. \tag{38}$$

This relation allows us to express the relative gain

variation $\delta K/K$ in terms of fluctuations in the coupling quality factor $\delta Q_c/Q_c$ and the quality factor of the active material $\delta Q_m/Q_m$:

$$\frac{\delta K}{K} = \frac{(K-1)(K+1)}{2K}\left(\frac{\delta Q_c}{Q_c} + \frac{\delta Q_m}{Q_m}\right). \quad (39)$$

For a given gain, greater bandwidth and increased stability can be obtained by using coupled cavities.[81]

The gain of a CPA is reduced sharply by a strong signal because of saturation effects. The dependence of gain on input signal power can be found[82] by assuming that the Q of the material is inversely proportional to the relative population difference $Z = (n_3 - n_2)/N$:

$$Q_m = \frac{a}{Z}, \quad (40)$$

where the quantity

$$Z = \frac{Z_0}{1+(3/2)W_{32}T_1} \quad (41)$$

is determined by the signal power through the probability of induced emission W_{32}. Relating the input signal power P_{in} to the value of W_{32} in terms of the loaded resonator Q we can find the gain K from (38)

$$K = \frac{K_0 + (K+1)(K_0-1)SP_{in}}{1+(K+1)(K_0-1)SP_{in}}, \quad (42)$$

where K_0 is the maximum gain of the CPA and

$$S = \frac{3}{4}\varkappa\frac{\mu_{32}^2}{\hbar^2}\frac{T_1T_2}{VA}.$$

Here, κ is the filling factor while V is the volume of the working material. The dependence of gain G (in decibels) on the product SP_{in} is shown in Fig. 18.

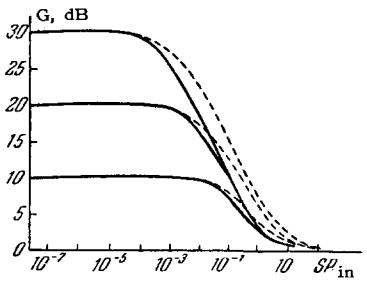

FIG. 18. Amplitude characteristic of paramagnetic amplifiers. The solid line refers to CPA while the dashed lines refer to the TWPA.

It should be pointed out that maximum gain is not reached immediately upon removal of the saturation signal; a finite time interval is required. The quantity τ_r, the time required to reestablish a gain $K < K_0$ after removal of a completely saturating signal, can be computed if we assume that the population difference is reestablished in accordance with the relation

$$Z = Z_0(1 - e^{-t/T_1}). \quad (43)$$

Thus, the time required to reestablish a gain level $K = 0.9K_0$ (i.e., a gain 1 dB below the maximum gain) is

$$\tau_r = T_1 \ln\frac{(0.9K_0+1)(K_0-1)}{0.2K_0}. \quad (44)$$

Because the system is regenerative the time required for reestablishing the gain is determined by the quantity K_0 in addition to the spin-lattice relaxation time T_1. The restoration time τ_r can be reduced by introducing a second paramagnetic ion, thereby increasing the relaxation probability for the $2 \longleftrightarrow 1$ transition (cf. Fig. 13).[59]

A basic advantage of microwave paramagnetic amplifiers is their low natural noise level. Many authors have analyzed the inherent noise in maser amplifiers.[3,83-87] The noise sources are the thermal radiation from the walls of the cavity and the spontaneous emission of the spin system in the inverted population state. At helium temperatures the effective microwave noise temperature is less than 10°K; this value has been verified experimentally.[88]

Because of the great importance of noise in maser amplifiers we shall consider this question in greater detail.

The noise properties of physical systems in thermodynamic equilibrium are described by the fluctuation-dissipation theorem of Callen and Welton.[89,90] Quantum-mechanical amplifiers, which are highly nonequilibrium systems, are characterized by a negative effective temperature; the value of the negative temperature is a measure of the inversion that is achieved. By definition this temperature is

$$T_e = \frac{h\nu}{k\ln\frac{n_1}{n_2}}, \quad (45)$$

where n_1 is the population in the lower energy level and n_2 is the population in the upper energy level. When the populations are inverted we have $n_1 < n_2$.

The temperature T_e applies only for the two energy levels between which transitions at the signal frequency take place. From the noise point of view we need consider only these two levels (even in many-level systems) because effects due to levels connected by the pump radiation are negligibly small in the frequency band close to the signal frequency.[3]

The Callen-Welton theorem can be generalized to the case of nonequilibrium stationary systems with negative effective temperatures: the spectral intensity of the fluctuations in these systems is determined by this temperature (more precisely, by the modulus of this temperature) and the value of the negative losses (cf.[91]). In a single-mode system the spectral density of the square of the fluctuating voltage $\overline{E_\nu^2}$ across a resistor R is

$$\overline{E_\nu^2} = 4Rh\nu\frac{1}{e^{h\nu/kT}-1}. \quad (46)$$

Since $R = -|R|$ and $T = -|T_e|$, Eq. (46) can be written in the form

$$\overline{E_\nu^2} = 4|R|h\nu\frac{e^{h\nu/k|T_e|}}{e^{h\nu/k|T_e|}-1}, \quad (46a)$$

where $|R|$ is the modulus of the negative resistance associated with the active material and $|T_e|$ is the

modulus of the negative temperature of the material. The relation we have written represents a generalization of the familiar Nyquist formula to the class of systems being considered here. This relation can be written in terms of the spectral density of the noise power

$$P_\nu = h\nu \frac{e^{h\nu/k|T_e|}}{e^{h\nu/k|T_e|} - 1}. \quad (47)$$

When $h\nu \ll k|T_e|$, corresponding to small inversion, i.e., the case $n_2 \gtrsim n_1$,

$$P_\nu = k|T_e|. \quad (47a)$$

In the case of total inversion, where $n_1 = 0$ so that $T_e = -0$,

$$P_\nu = h\nu. \quad (47b)$$

The relations in (46a), (47), (47a), and (47b) describe the noise due to spontaneous emission of the inverted spin system in quantum-mechanical amplifiers.

If N modes can be excited in the quantum-mechanical amplifier the relations we have obtained must be multiplied by N. In particular, if the volume density of field oscillators is the same as for free space, the energy density of the spontaneous radiation u_ν is given by

$$u_\nu = 4\frac{\nu^2}{c^3} h\nu, \quad (48)$$

in which we recover the well-known relation showing that the energy density of spontaneous radiation is proportional to the cube of the frequency.

Another noise source besides spontaneous emission is the noise due to the thermal radiation from the walls of the quantum-mechanical amplifier. This noise is very weak at helium temperatures. From a knowledge of the spectral composition of the fluctuation radiation in the quantum-mechanical amplifier we can determine the spectral density of the input noise, i.e., the noise factor; however, a quantity more convenient in the microwave region is the effective temperature of the input noise.

In a reflection-cavity microwave paramagnetic amplifier the effective temperature is (at high gain)[83]

$$T_{in} = T_e + T_0 + \frac{Q_c}{Q} \approx T_e, \quad (49)$$

where T_0 is the temperature of the cavity walls. This quantity is less than a few degrees Kelvin. Similarly, in a traveling-wave amplifier (cf. below) we find[92]

$$T_{in} = T_e + (T_0 + T_e)\frac{\alpha_g}{\beta - \alpha_g}, \quad (50)$$

where α_g is the absorption coefficient of the waveguide walls while β is the negative absorption coefficients of the active material (both per unit length of the traveling-wave amplifier). The quantity T_{in} is again a small quantity.

The use of low-noise paramagnetic amplifiers can make possible an appreciable improvement in the sensitivity of microwave receivers. However, one must distinguish between the inherent sensitivity of a paramagnetic amplifier and the sensitivity of a receiver in which a paramagnetic amplifer is used. The first quantity is extremely large. The second, however, is determined to a large extent by the noise from cosmic sources, atmospheric noises, and noise in the antenna line.

It is easy to find the improvement in the sensitivity of a microwave detection system using a CPA designed for the reception of monochromatic signals.[93] The ratio of the minimum detectable intensity without the CPA, P_0, to the minimum detectable intensity with the CPA, P, is given by

$$\frac{P_0}{P} = \frac{T_a + \frac{N}{1-\alpha_f} T_0}{T_a + \frac{\alpha}{1-\alpha} T_0}. \quad (51)$$

Here, T_a is the effective temperature of the antenna, N is the noise factor of the receiver, T_0 is the temperature of the surrounding medium, α_f is the absorption coefficient of the antenna feeder system, and $\alpha = \alpha_f + \alpha_c - \alpha_f\alpha_c$ is the absorption coefficient of this system when the CPA is not used. The difference between α and α_f is due to the loss in the ferrite circulator α_c; an isolator must be used in a reflection CPA in order to isolate the input and output of the amplifier.

The relation in (51) holds if the gain of the CPA is high enough. In this case the noise generated in the later parts of the receiver does not contribute to the noise factor. If this situation is to obtain it is necessary that $K^2 \gg N/\alpha$. Under typical conditions in the centimeter region for observations at small angles with respect to the horizon the relation in (51) yields a ten-fold improvement in sensitivity. At larger angles the improvement factor can be as high as fifty.

Thus, we see that the use of a CPA preamplifer in a receiver designed for the reception of coherent signals yields a marked improvement in receiver sensitivity.

Noise receivers, for example, the receivers used in radio astronomy, require a more careful analysis. The sensitivity of these devices increases with bandwidth. For this reason, the use of a CPA, which can reduce bandwidth in addition to reducing the effective temperature of the input signals, need not necessarily mean an improvement in radiometer sensitivity. Thus, the relation in (36) should be recalled in evaluating the sensitivity of a CPA radiometer.[93,94] It is evident that there is an optimum value of the gain, at which the sensitivity is highest. A higher gain means a lower effective noise temperature but also means a narrower bandwidth. By applying the usual techniques[95] to a CPA radiometer one easily finds that the sensitivity is optimized when the power gain $G = K^2 = 4.5\,T''/T'$ and the bandwidth of the receiver following the CPA preamplifier $\Delta\nu_2 = 3A\sqrt{T'/T''}$. Here, T″ and T′ are the effective noise tempera-

tures at the output and input of the CPA respectively. If these conditions are satisfied, in a radio-astronomy measurement of a low-temperature source with a low-loss circulator the improvement in sensitivity in terms of antenna temperature is

$$\frac{\delta T_{a_0}}{\delta T_a} = 0.7 \left(\frac{N}{\alpha_f}\right)^{3/4} \sqrt{\frac{A}{\Delta\nu}}, \quad (52)$$

where $\Delta\nu$ is the bandwidth of the receiver used as a radiometer without the CPA.

Thus, the CPA is especially useful in radio astronomy receivers if one can achieve the required gain-bandwidth product without reducing the bandwidth of the receiver used in the radiometer without the CPA. It should be kept in mind, however, that a CPA with an amplifier providing more than 20 dB of gain can be unstable.

2. Traveling-wave paramagnetic amplifier (TWPA). Now consider the case in which the active material is placed in a waveguide along which the amplified radiation is propagated in the form of a traveling wave; because the absorption due to the active material is negative, the radiations intensity grows exponentially. The energy flux P propagated along the system (with group velocity v_{gr}) is related to $|Q_m|$ by the expression

$$\frac{dP}{dx} = \frac{2\pi\nu P}{v_{gr}|Q_m|}. \quad (53)$$

It then follows that the power gain of the TWPA is [96]

$$G = \exp\left\{2\pi \frac{mn}{|Q_m|}\right\}, \quad (54)$$

where $m = c/v_{gr}$ is the reduction factor giving the group velocity and $n = l/\lambda_0$ (λ_0 is the free-space wavelength while l is the length of the TWPA). The gain in decibels is given by

$$G = 27.2 \frac{mn}{|Q_m|} \text{ [dB]}. \quad (54a)$$

The bandwidth of the TWPA is determined by the shape of the absorption line. If this shape is Lorentzian the dependence of TWPA gain on frequency is given by

$$G_{(dB)}(\nu) = G^0_{(dB)} \frac{\Delta\nu_l^2}{\Delta\nu_l^2 + x^2}, \quad (55)$$

where $\Delta\nu_l$ is the half-width of the resonance absorption line while x is the deviation from the resonance frequency. It is evident that the bandwidth of the TWPA is determined by the width of the absorption line and that it is a much weaker function of the achievable gain. In particular, the bandwidth of the TWPA at the 3 dB level is

$$\Delta\nu = 2\Delta\nu_l \sqrt{\frac{3}{G^0_{(dB)} - 3}}. \quad (56)$$

In contrast with the CPA, the gain and bandwidth of the TWPA are independent of frequency, inasmuch as the line width is essentially independent of frequency. For this reason the use of a TWPA can yield an especially large increase in the relative bandwidth of a receiver at low frequencies.

The TWPA is also more stable because there are no regeneration instabilities. The relative gain variation due to fluctuations in the Q of the active material is given by

$$\frac{\delta G}{G} = \ln G \frac{\delta Q_m}{Q_m}. \quad (57)$$

It should be noted that the TWPA is free from regenerative instabilities only so long as it exhibits unidirectional gain and only amplifies the radiation propagating from input to output. To avoid the deleterious effects of unavoidable reflections the TWPA must provide unidirectional absorption of the backward wave; the backward wave must be reduced by a factor of L, where

$$L \gg G\Gamma_1\Gamma_2,$$

where Γ_1 and Γ_2 are the power reflection coefficients at the input and output.

The nonreciprocal gain and attenuation in the TWPA are usually achieved by introducing a region in which the microwave magnetic field is circularly polarized with opposite polarizations for the forward wave and the backward wave. The backward wave can be absorbed by a ferrite located in a region of appropriate circular polarization or by the same paramagnetic material used for providing gain; in the latter case the concentration is much higher, in which case the absorption at the signal frequency remains essentially unchanged by the pump radiation. It follows from (54) that to obtain any appreciable gain using conventional lines in a traveling-wave system the system must be several meters long; this is essentially impossible in practice. For this reason it is necessary to make use of a slow-wave structure. [96,97]

The amplifier saturates at high input levels. The dependence of TWPA gain on input signal power is determined by the input-power dependence of Q_m. Using the relation between Q_m and P_{in} we can write (53), the energy flux relation, in the form

$$\frac{dP}{dx} = \frac{AP}{1 + SP} \quad (58)$$

where A is the gain, while S is the saturation factor which, as in the case of the CPA, is proportional to T_2T_1. The relation in (58) then gives the desired expression

$$G = G_0 e^{-SP_{in}(G-1)}.$$

The general nature of this relation is the same as for the CPA except that it is much sharper for a given value of S (Fig. 18).

The time required to restore the gain of a TWPA after the saturation signal is removed is given by

$$\tau_m = T_1(1.5 + \ln\ln G_0). \quad (59)$$

As we have indicated above, the inherent noise of a

microwave TWPA is negligibly small. For this reason the use of a TWPA preamplifier in a receiver for coherent signals affords an improvement in sensitivity given by same relation as in the case of the CPA. The TWPA, however, does not require a circulator so that in practice $\alpha = \alpha_f$. The use of a TWPA in a noise receiver also gives a very important improvement. This question has been considered in detail in [93]. In Fig. 19 we show curves characterizing the improvement (in decibels) in radiometer sensitivity that can be obtained. The dotted curve refers to a radiometer with a CPA while the solid curves refer to a radiometer with a TWPA with gain of 10, 20, and 30 dB. In this same figure the dashed curve shows the optimum CPA gain required for achieving the biggest improvement in sensitivity.

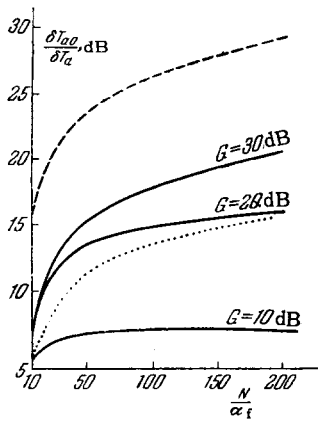

FIG. 19. Improvement in sensitivity of a radiometer using paramagnetic amplifiers.

3. Experimental results. The first paramagnetic amplifier made use of the Gd^{3+} ion in lanthanum ethyl sulfate $La(C_2H_5SO_4) \cdot 9H_2O$.[59] In some of the earliest work use was also made of potassium cobalticyanide $K_3Co(CN)_6$ doped with Cr^{3+}.[98]

At the present time the material most widely used in microwave maser amplifiers is chromium corundum (ruby); the EPR spectrum and the relaxation properties of this material have been described above. Maser amplifiers using this material have been built for wavelengths ranging from 3 cm to 1 m.[99-102] At higher frequencies ($\lambda = 8$ mm and $\lambda = 1.25$ cm) use is made of the Cr^{3+} and Fe^{3+} ions in rutile TiO_2.[103,30] The Fe^{3+} ion has also been used in corundum Al_2O_3 in amplifiers designed for the 3 cm[25] and 10 cm[104] ranges. Most of the maser amplifiers that have been described at the present time make use of ruby. With these amplifiers it has been possible to achieve a substantial improvement in sensitivity in radio telescopes operating at 3 cm and 21 cm[94,105] and to increase the sensitivity of 3-cm radar systems by 11 dB.[106]

Most of the paramagnetic amplifiers presently in use are of the cavity type. In these amplifiers the cavity is tuned to the signal frequency and the pump frequency simultaneously. In the 10-centimeter range a two-frequency cavity acts as a coaxial cavity at the signal frequency and a conventional waveguide cavity at the pump frequency. The coaxial cavity configuration is realized by means of capacity-loaded segments of coaxial line[107,108] or strip-line segments.[59,109]

The coaxial cavity is usually excited by means of an appropriate rod or coupling loop that is an extension of the coaxial line. In Fig. 20 we show a schematic diagram of a strip-line CPA.[109] At shorter wavelengths, starting at $\lambda = 3$ cm, it is more convenient to use volume cavity resonators in which the signal frequency and pump frequency correspond to higher modes. A cavity resonator of this kind[99] is shown in Fig. 21. The same approach is used at still higher frequencies. A dielectric resonator has been used at 8 mm; in this case the dielectric material, which has a

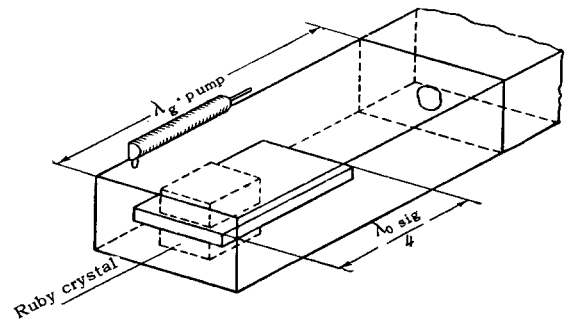

FIG. 20. Strip-line resonator.

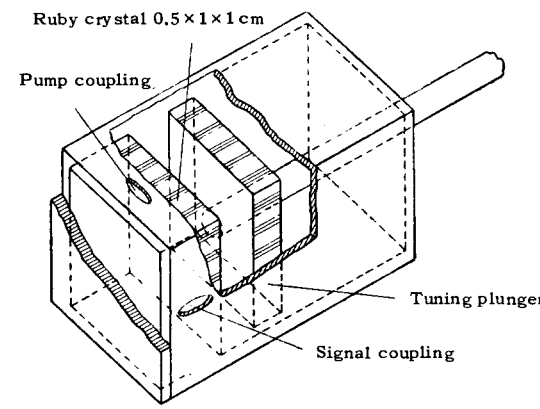

FIG. 21. Cavity resonator.

high dielectric constant ($\epsilon_\perp = 120$, $\epsilon_\parallel = 220$ at 4.2°K [103]), is also the working material (rutile). In the 10-centimeter range most amplifiers make use of the energy levels of the Cr^{3+} ion in Al_2O_3 with the perpendicular orientation, in which case the external magnetic field is perpendicular to the trigonal axis of the crystal. A diagram showing the energy levels for this orientation has been given in Fig. 3. Two different modes of operation are possible. At lower fields signal amplification is obtained by using transition between levels 1 and 2 while the pump radiation is applied between levels 1 and 4. A feature of this mode of operation is the low magnetic field (200—700 Oe

for λ = 30—10 cm) and the weak dependence of pump frequency on signal frequency (λ = 2.25—2.5 cm for the signal range λ = 10—30 cm). However, better results are obtained at higher fields, in which case gain is obtained by using the 3—4 transition while the pump radiation corresponds to the 2—4 transition. Thus, in a field H ≈ 3000 Oe with pump radiation at λ = 2.15 cm it has been possible to obtain a gain-bandwidth product A = 55 Mc at 10 centimeters.[108] Still better results may be expected in this mode of operation with pump radiation at λ = 1.2 cm, corresponding to the 1—4 transition.

At wavelengths below 5 cm it is possible to use the so-called "symmetric" or "push-pull" mode of operation. This mode can be used when the external magnetic field is at an angle $\theta = 54°44'$ with respect to the trigonal axis of the crystal. Under these conditions the energy levels are symmetric about the abscissa axis (Fig. 2). If the signal is applied between levels 2 and 3, the pump radiation at frequency $\nu_{13} = \nu_{24}$ simultaneously depletes level 2 and enriches level 3. The advantage of this mode of operation has already been discussed. The symmetric mode has been used at λ = 3 cm with pump radiation at λ = 1.27 cm and a magnetic field of the order of 4300 Oe. It was possible to obtain a gain-bandwidth product of the order of 100 Mc.[94,99,110]

Chromium corundum has been used in traveling wave amplifiers[96] as well as cavity amplifiers. A TWPA has been built at λ = 5.2 cm using pump radiation at λ = 1.6 cm. A bandwidth of 25 Mc was obtained with a gain of 23 dB. A vane slow-wave structure was used. The ruby was placed at the base of the vanes, at nodes of the magnetic field. The high bandwidth of the slow-wave structure made it possible to tune the TWPA over a range of 350 Mc by electronic tuning. The slow-wave structure was coupled to the input coaxial line by means of a vane structure. In Fig. 22 we show a TWPA with the vane slow-wave structure with direct coupling to the input signal waveguide.[97]

It is of interest to note that presently available maser amplifiers operating at liquid helium temperatures need not require large magnets. Electromagnets and solenoids have been developed which can be immersed in liquid helium.[111] The winding is made from niobium wire, which remains a superconductor

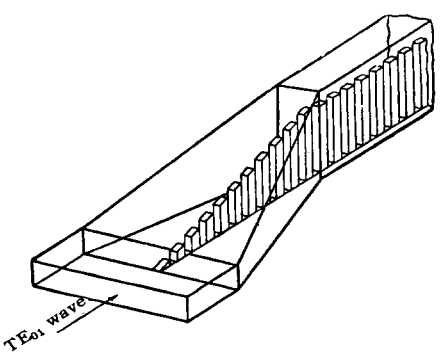

FIG. 22. Ridge structure used for slow-wave system.

at rather high fields. A field of 4300 Oe has been obtained with a superconducting solenoid and fields up to 14,000 Oe have been obtained in core magnets with superconducting windings. These magnets are small in size and extremely stable.

We may also note that a CPA has been operated in the 3-cm region at liquid oxygen temperature 60°K (evacuated).[112]

V. QUANTUM-MECHANICAL OPTICAL OSCILLATORS AND AMPLIFIERS (OPTICAL MASERS)

Because of the high degree of success achieved in the development of microwave maser devices it was natural to investigate the possibility of extending this development to much shorter wavelengths. The problem of building oscillators and amplifiers for the submillimeter region has been discussed in [113] while devices for the optical region have been discussed in [114].

Optical masers have been built using the Cr^{3+} ion in Al_2O_3[115,116] and the U^{3+} and Sm^{3+} ions in CaF_2.[117,118]* The energy levels of the Cr^{3+} ion have been considered above and are shown in Fig. 8. Ruby has two absorption bands in the visible region. From these bands, in a time of approximately 2×10^{-7} sec there are nonradiative transitions to the $\overline{2A}(^2E)$ and $\overline{E}(^2E)$ levels. Since the probability for nonradiative transitions from the $\overline{2A}(^2E)$ and $\overline{E}(^2E)$ levels is small, transitions from these levels to the lower level occur by virtue of spontaneous emission, in a time of approximately 5×10^{-3} sec. The long lifetime of these levels stems from the fact that the electric dipole transitions are highly forbidden. This radiation is observed in the red region and corresponds to the wavelengths 6929 Å (R_2 line) and 6940 Å (R_1 line). Irradiation by green light causes the populations to increase in the $\overline{2A}(^2E)$ and $\overline{E}(^2E)$ levels.

A situation can arise in which the population of some one of these levels is greater than the population in the ground (lower) level. It is difficult to obtain a negative temperature in this level scheme because at the outset the entire population is in the lower level of the two levels between which a negative temperature is desired. Consider the conditions for obtaining a negative temperature between levels 1 and 3 (Fig. 23) where level 1 is the lower level. The pump radiation is applied between levels 1 and 2. Nonradiative transitions take place from level 2 to level 3. Spontaneous emission occurs between level 3 and level 1. We introduce the following notation: $W_{12} = W_{21}$ is the probability of a transition from level 1 to level 2 and vice versa under the effect of the pump radiation, w_{21} is the probability of relaxation transitions from level 2 to level 1, w_{23} is the probability for relaxation

*Optical masers have also been built with gas mixtures as the working material. An optical maser using a discharge in a mixture of the He and Ne is described in [119].

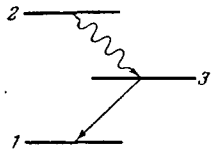

FIG. 23. Three-level optical maser.

transitions from level 2 to level 3, w_{31} is the probability for spontaneous emission from level 3 to level 1. We also assume that w_{12} and w_{32} are so small that they can be set equal to zero. In addition we neglect relaxation transition between levels 3 and 1.

At thermal equilibrium the entire population is in the lower level and we denote the total population by n. The pump radiation causes a distribution of population over all three levels; the populations of the three levels are denoted by n_1, n_2, and n_3 respectively. The kinetic equations describing the populations in the levels are written in the form

$$\left.\begin{aligned} \frac{dn_1}{dt} &= (n_2 - n_1) W_{12} + n_2 w_{21} + n_3 w_{31}, \\ \frac{dn_3}{dt} &= n_2 w_{23} - n_3 w_{31}, \\ n_1 + n_2 + n_3 &= n. \end{aligned}\right\} \qquad (60)$$

In the stationary state we must have $dn_i/dt = 0$. The population difference for levels 3 and 1 is then

$$n_3 - n_1 = -n \frac{W_{12}(w_{31} - w_{23}) + w_{31}(w_{21} + w_{23})}{W_{12}(2w_{31} + w_{23}) + w_{31}(w_{21} + w_{23})}. \qquad (61)$$

We now consider several particular cases:

1. $W_{12} \gg w_{ik}$; $n_3 - n_1 = n \frac{w_{23} - w_{31}}{2w_{31} + w_{23}}$.

It is clear that the condition $n_3 > n_1 > 0$ can be satisfied if $w_{23} > w_{31}$. If $w_{23} \gg w_{31}$, then $n_3 - n_1 \approx n$, $n_1 \approx 0$.

2. If W_{12} is finite, then $n_3 - n_1 > 0$ when

$$W_{12} > \frac{w_{31}(w_{21} + w_{23})}{w_{23} - w_{31}}.$$

If $w_{23} \gg w_{31}$, this condition reduces to $W_{12} > w_{31}$.

Thus, the necessary condition for obtaining a negative temperature between levels 1 and 3 is

$$w_{23} > w_{31}. \qquad (62)$$

If $w_{23} \gg w_{31}$ the required pump power must be such that the probability of a transition from level 1 to level 2 is greater than the probability of spontaneous emission from level 3 to level 1. In ruby $w_{23} \approx 2 \times 10^{-7}$ sec and $w_{31} \approx 5 \times 10^{-3}$ sec so that the condition in (62) is easily satisfied. The level system considered here differs from the level system in ruby in that the single 3 level is replaced by two levels, which are 30 cm^{-1} apart. The time for establishing thermal equilibrium between these two levels is shorter than the time required for spontaneous emission. This situation holds down to helium temperatures. Hence it may be assumed that the distribution of population between the $\bar{E}(^2E)$ and $\overline{2A}(^2E)$ levels is a Boltzmann distribution. From a knowledge of the total population of these levels it is then possible to determine the population in a given level.

It is clear that with all other conditions equal the production of a negative temperature between a ground state and an excited state requires more pump power than that required for a negative temperature between two excited states. A level system of the latter kind is exhibited by U^{3+} in the CaF_2 lattice and by Sm^{2+} in the same lattice. The spectra of these ions in CaF_2 have been studied in [131,132].

We first consider the condition for obtaining a negative temperature between levels 3 and 4 in the level system shown in Fig. 24. The pump radiation is applied between levels 1 and 2 and the probability of a transition under the effect of this radiation is denoted

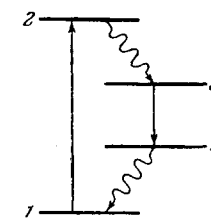

FIG. 24. Four-level optical maser.

by w_{12}. There are nonradiative transitions from level 2 to level 3, with probability given by w_{23}. Transitions from level 3 to level 4 can only occur by spontaneous emission, with probability w_{34}; finally, transitions from level 4 to level 1 are characterized by the probability w_{41}. It is assumed that the temperature is so low that the quantity w_{14} can be neglected. Forming the equation for the populations in these levels, following the procedure used above, we obtain the condition for a negative temperature between levels 4 and 3:

$$w_{41} > w_{34} + \frac{w_{24}}{w_{23}}(w_{34} + w_{31}). \qquad (63)$$

Usually w_{23} is large compared with the other probabilities. If this situation holds the condition in (63) reduces to the condition

$$w_{41} > w_{34}. \qquad (64)$$

Thus, the probability of a transition from level 4 to level 1 must be greater than the probability of spontaneous emission. It is only when this condition is satisfied that a negative temperature can be obtained between these levels. The transition probability due to the pump radiation does not appear in (63). This means that a negative temperature can be obtained with an arbitrarily small pump power. In practice, however, this is not the case because in the initial state the population of level 4 is never zero. This initial population then determines the threshold pump radiation and the threshold can be reduced by using low temperatures.

A negative temperature represents a necessary, but not sufficient, condition for obtaining oscillation or amplification. The excess population in the upper level must be large enough to compensate for all losses.

The material must be placed in a cavity resonator to produce oscillations. In the microwave region one usually uses cavity resonators whose dimensions are comparable with the wavelengths of interest. However, at very short wavelengths the resonator dimensions would be so small that it would be impossible to fabricate them. A new kind of submillimeter resonator has been proposed in [113]; the dimensions of this resonator are much greater than the wavelengths at which it operates. This resonator has been used experimentally in the millimeter region.[120] The possibility of using a resonator of this type in the optical region has been investigated in detail in [114]. This resonator was, in fact, used for the first optical masers.[115,119]

The resonator consists of two parallel reflecting plates separated by a distance l. The dimensions of the plates are much greater than the wavelength excited in the resonator λ. The Q of the resonator is[113,120]

$$Q=\frac{2\pi l}{\lambda}\frac{1}{1-K}, \tag{65}$$

where K is the reflection coefficient of the plates. It may be assumed that a plane wave is excited between these plates and that the loss is determined by the reflection coefficient itself. Diffraction losses can be neglected if the plates are large enough. The effect of the reflecting surfaces is essentially to increase the path length transversed by the plane wave, l, by a factor $1/(1-K)$. If $K = 0.95$ the path length is increased twenty times, that is to say, the wave decays by a factor of e in 20 reflections. It should be noted that the resonance condition is satisfied when the propagation path between the plates comprises an integral number of half-wavelengths.

In addition to the wave that propagates perpendicularly to the surface of these plates, there are other waves that propagate almost perpendicularly. Consider a plane wave propagating at some angle and reflected $1/(1-K)$ times; before long it will move beyond the edges of the plates. Assume that this mode has a Q one half that of the case in which wave propagation is strictly normal to the plates.

The corresponding limiting angle is then

$$\theta=\frac{D(1-K)}{l}. \tag{66}$$

The maximum path length between the plates l'_M is then

$$l'_M=\frac{l}{\cos\theta}\approx l\left(1+\frac{\theta^2}{2}\right), \tag{67}$$

and consequently

$$l'_M-l\approx l\frac{\theta^2}{2}. \tag{68}$$

The number of additional half-wavelengths r along the path l'_M is

$$r=\frac{l\theta^2}{\lambda}=\frac{D^2(1-K)^2}{\lambda l}. \tag{69}$$

If $D = l = 1$ cm, $\lambda = 10^{-4}$ cm, $1-K = 0.05$ then $r = 25$. Thus, there are 25 different angles $< \theta$ for which a plane wave can be propagated in such a way that there will be an integral number of half-wavelengths between the plates. To determine the number of half-wavelengths between the plates we introduce a coordinate system x, y, z whose xy plane coincides with one of the plates. We now introduce the wave vector K

$$K^2=K_x^2+K_y^2+K_z^2. \tag{70}$$

When $K_y^2 = 0$, $K_X^2 = K^2 - K_Z^2$. Assuming that $K_X = \pi S/D$, where S is an integer, and substituting the value of θ from (66) we have

$$S=\frac{D^2(1-K)}{\lambda L}. \tag{71}$$

If $D = L = 1$ cm, $\lambda = 10^{-4}$ cm, $1-K = 0.05$ we find $S = 500$. Proceeding in this way we can find the modes that will be excited in the resonator and determine the number of such modes. However, the number of possible resonator modes can be determined in another way if we assume that the resonator dimensions are much greater than a wavelength. In this case the total of modes in a volume V is

$$N'=\frac{8\pi V\nu^2\Delta\nu}{c^3}. \tag{72}$$

Of this total number of modes the only ones with high Q's will be those whose direction of propagation lies in a solid angle $d\Omega = \pi\theta^2$, where θ is determined from (66). The number of such modes is

$$\alpha=\frac{8\pi^2\nu\,|\mu|^2\Delta n}{hc\,\Delta\nu}, \tag{73}$$

If $D = L = 1$ cm, $1-K = 0.05$, $\lambda = 10^{-4}$ cm, $\Delta\nu/\nu = 10^{-4}$ then $N'' \approx 10^7$.

A paramagnetic crystal can also be used directly as a resonator. It is then fabricated as a cylinder whose end faces are plane-parallel and silvered. This cylinder is a cavity resonator. The crystal is irradiated by the pump radiation through the lateral surface.

The propagation of a wave in the crystal can be characterized by two quantities: the negative absorption coefficient α, associated with the negative temperature, and the absorption coefficient α_{cl} associated with the loss in the crystal itself. The negative absorption coefficient is given by

$$N''=\frac{\pi^2D^4(1-K^2)}{2c^3l}\nu^2\Delta\nu, \tag{74}$$

where ν is the frequency, μ is the matrix element of the dipole transition, h is Planck's constant, c is the velocity of light, $\Delta\nu$ is the width of the spectral line and Δn is the excess population in the upper level. If $\alpha > \alpha_{cl}$ the wave energy increases in accordance with the relation $\exp\{(\alpha-\alpha_{cl})l\}$. Energy is lost when the wave is reflected from the surface. If this loss is smaller than the energy acquired in the path length l the self-excitation condition is satisfied. Thus, the self-excitation conditions can be written in the form

$$Ke^{(\alpha-\alpha_{cl})l} > 1. \quad (75)$$

This condition can also be written in the form

$$K'e^{\alpha l} > 1, \quad (75a)$$

where $K' = Ke^{-\alpha_{cl}l}$, that is, the effect of absorption in the material is equivalent to a reduction of the reflection coefficient by a factor $e^{\alpha_{cl}l}$. If $\alpha l \ll 1$, (75a) is written in the form

$$\frac{K'}{1-K'}\alpha l > 1. \quad (75b)$$

This condition can be satisfied if $K' \approx 1$. Substituting α from (74) in (75b) we can write the self-excitation condition in the form

$$\frac{8\pi^2 l\nu\,|\mu|^2\,\Delta n}{hc\,(1-K')\,\Delta\nu} > 1. \quad (76)$$

It should be noted that (76) cannot be used if K is appreciably different from unity. The relation in (75) must be used in this case. The relation in (76) also describes absorption in the absence of inversion. In this case Δn is taken to mean the excess population in the lower level. The absorption coefficient in ruby for the R_1 line has been measured in [32] in a fixed magnetic field at 77°K and found to be 13 cm^{-1}. If we substitute the populations of the lower and upper levels the negative absorption is also 13 cm^{-1}. If $l = 1$ cm, the self-excitation condition (76) is satisfied if the reflection coefficient $K' > e^{-13}$ or $K' > 10^{-6}$, that is to say, by a negligible reflection coefficient. In practice, however, it is impossible to achieve this strong an inversion.

1. Optical masers using ruby and fluorite. An optical maser using ruby as the paramagnetic crystal, with a chromium concentration of approximately 0.05%, has been described in [115] and [116]. The ruby crystal described in [116] is 0.5 cm in diameter and the end faces are parallel to an accuracy of 1′. The faces were silvered in such a way that one face could transmit from 1 to 5% of the incident light, thus providing a means for emitting the radiation. The pump radiation was produced by a flash lamp supplied from a 400 μF capacitor bank charged to 4 kV. The pulse length was 5×10^{-4} sec. The radiation was detected with a photomultiplier. The time constant of the detection apparatus was 10^{-6} sec. At excitation levels lower than the critical value the intensity ratio of the R_1 and R_2 lines is approximately unity (the crystal temperature T = 300°K). At discharge energies greater than 2,000 J, the intensity ratio R_1/R_2 is increased by three orders of magnitude as viewed through the semi-transparent face. The radiation emitted through the lateral wall is not changed and the intensity ratio is approximately unity. The coherent radiation consists of individual pulses. The time interval between pulses is several microseconds.

The shortest time intervals between pulses are observed at high excitation levels. The radiation pulses are approximately 5×10^{-7} sec in length. The fact that the radiation is produced in bursts indicates that self-excitation leads to a rapid loss of population from the upper level, thereby ending the radiation process and quenching the oscillations. After a finite time interval the population again accumulates in the upper level and the self-excitation condition is satisfied. [122] It must be emphasized that this effect may also be due to the excitation of different modes in the resonator. [123] The threshold excitation power is reduced by 30% when the ruby is cooled to liquid nitrogen temperature (77°K).

The quality of the crystals was investigated by x-ray methods. The variation in the direction of the axis along the length of the crystal was ±1°. Thus, the optical path length between the crystal faces can vary by several wavelengths. The peak radiation power was approximately 10 kW and the effective radiation temperature was 10^{10} degrees. Under self-excitation conditions the line is narrowed to 0.2 cm^{-1} (the initial width is 6 cm^{-1}). The oscillator efficiency is approximately 1%. The directivity of the radiation beam is approximately 0.2°. An optical maser using ruby with a higher Cr^{3+} concentration, approximately 0.5%, has been described in [121,125]. At this concentration in ruby some of the chromium ions in the lattice are very close to each other, forming pairs which are coupled by an exchange interaction; this effect leads to the appearance of new energy levels and luminescence lines. [125-127] In particular, lines appear at wavelengths 7009 Å (N_2) and 7041 Å (N_1). The N_1 and N_2 lines exhibit good fluorescence but weak absorption and the absorption disappears at low temperatures. These effects are explained by the fact that the lower level for these transitions is not the ground state, but lies approximately 100 cm^{-1} above the ground state. It is interesting to note that the energy of the excited single ions is transferred efficiently to the ion pairs. The ruby is in the form of a rod 2 mm in diameter and 4 cm long with the faces treated in the same way as those described above. The experiments were carried out at liquid nitrogen temperature. The pump radiation was produced by a xenon lamp supplied from a condenser bank of 400 μF. Self-excitation was obtained for the N_1 line (7041 Å) at 3500 V. The N_2 line (7009 Å) was also excited when the voltage was raised to 3700 V. The directivity of the radiation beam was approximately 1°.

The simultaneous excitation of the two lines (N_1 and N_2) is due to the fact that the upper levels of the corresponding transitions are different and that the time required to establish thermal equilibrium between these lines is greater than the spontaneous emission time. This interpretation is supported by the fact that the relative intensities of these lines change from sample to sample in random fashion. The required pump power is approximately the same as in ruby with a concentration of 0.05%. It is to be expected that this quantity would be appreciably smaller

for operation at 4°K, in which case the lower level is weakly populated.

A maser for the infrared region (2.5μ) has been described in [117]. In this case CaF_2 was doped with U^{3+}. The techniques for growing this crystal and the energy levels are described in [131]. The level diagram for U^{3+} is shown in Fig. 25. This crystal has strong absorption bands in the green and blue. The uranium ions excited in these bands make nonradiative transitions to two metastable levels separated by 120 cm^{-1}. The luminescence spectrum consists of 4 lines, with the lines at the longest wavelengths associated with the transition to the excited level approximately 515 cm^{-1} above the ground state.

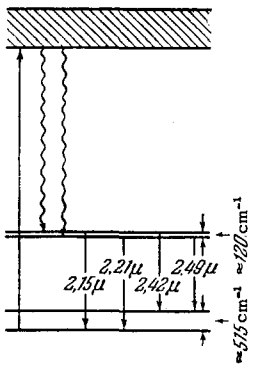

FIG. 25. Optical transitions of U^{3+} in CaF_2.

The fluorite crystal, with a uranium concentration of 0.05%, was fabricated in the form of a cylinder approximately 1 cm in diameter and 4 cm in length. The cylinder faces were polished until plane to an accuracy of $1/20$ of a wavelength of the sodium line and were parallel to within 15″. The faces were silvered and covered with a film of SiO_2 to prevent oxidation of the silver layer. One face had a transmission factor of about 1.5%. The crystal was cooled without being in direct contact with the liquid helium and the crystal temperature was maintained in the range between 10 and 30°K. The source of pump radiation was a pulsed xenon lamp. The pump power required in this case is much smaller than for the ruby maser because the lower level of the transition is an excited state and is very weakly populated at low temperatures. The divergence of the radiation beam was approximately 0.5°. Here, as in the ruby case, the radiation is produced in bursts. Finally, in [118] an optical maser is described in which the Sm^{2+} ion (concentration 0.1%) is used in CaF_2. The level diagram for this crystal is given in Fig. 26. The radiation is observed at 7082 Å. This radiation is associated with induced transitions from the metastable level lying 14,500 cm^{-1} above the ground state to a level lying 369 cm^{-1} above the ground state. The crystal was cooled to 10—30°K. In contrast with the optical masers described above, the radiation produced in this case was continuous rather than in the form of bursts. This is probably due to the fact that the energy interval between the absorption band and the metastable level is small.

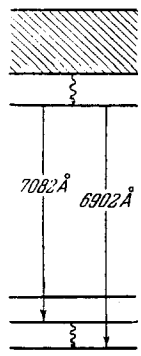

FIG. 26. Optical transitions of Sm^{2+} in CaF_2.

The radiation from an optical maser can be focused on an area with dimensions of the order of a wavelength. Under these conditions the field intensity at the focal point can be estimated from the relation

$$E \sim \frac{1}{\lambda}\sqrt{\frac{4\pi P}{c}}. \qquad (77)$$

If the peak radiation power density is P = 10 kW/cm^2 and $\lambda = 10^{-4}$ cm then $E = 2 \times 10^7$ V/cm.

Masers are characterized by a high degree of radiation coherence. The radiation emitted from different portions of the radiating surface exhibits a constant phase difference. Consequently it should be possible to obtain an interference pattern from two different points of this surface. None of the optical sources available at the present time possess this property. The radiation coherence of quantum-mechanical oscillators stems from the properties of induced emission. The frequency, polarization, phase, and direction of propagation of the induced-radiation photon are identical with those of the primary photon.

2. Maser amplifiers. Just as in the case of the microwave maser, the optical maser can be realized in the form of a traveling-wave amplifier or in the form of a cavity amplifier. Because present optical technology does not provide systems with high retardation, the required gain in a traveling-wave system is obtained by increasing the path traversed by the light in the crystal. If the negative absorption coefficient is α while the losses in the crystal are characterized by the absorption coefficient α_{cl}, the power gain K over a path of length l is

$$K = e^{(\alpha - \alpha_{cl})l}. \qquad (78)$$

The use of a cavity-resonator amplifier instead of a traveling-wave amplifier is equivalent to increasing the path length traversed by the light by $1/(1-K')$ times, where K′ is determined from (75a). Consequently, a resonator amplifier can be small in size.

In contrast with the microwave case, in the optical region the pump power required for saturation cannot be achieved; for this reason fluctuations in pump power cause changes in α because of the variation in the ex-

cess population in the upper level (74) and in turn these cause the gain to vary.

We now consider the stability of an optical maser amplifier assuming that fluctuations in the pump radiation can be neglected. [77]

The Rayleigh-Jeans law does not hold in the optical region. The spectral density of the thermal radiation is a nonlinear function of temperature. For this reason it is not useful to characterize the sensitivity of quantum mechanical amplifiers in terms of an effective temperature. Rather, one uses a minimum detectable spectral density of thermal radiation, or a minimum detectable intensity of monochromatic radiation.

Although the inherent noise of a quantum-mechanical amplifer is negligibly small in the microwave region, in the infrared or optical regions one must consider noise due to spontaneous emission. The spectral density of spontaneous emission associated with a single mode is given by (46). If there are N modes this spectral density is increased by N times:

$$P_{\nu}^{\text{spont}} = Nh\nu. \tag{79}$$

In the optical region, however, one can neglect the thermal radiation of the walls of the cavity as compared with the noise due to spontaneous emission.

In addition to the useful signal, at the input of the quantum-mechanical amplifier there will always be thermal radiation from the external medium, comprising a background against which the signal must be isolated. Hence, in analyzing the sensitivity of a quantum-mechanical receiver one cannot neglect the external background noise, whose effective temperature can, in general, be large. Since the spectral density of the noise being considered at the input of the amplifier is

$$P_{\nu} = Nh\nu + P_{\nu}^{b}\ , \tag{80}$$

the output noise power is given by

$$P_{\text{out}} = G\,\Delta\nu_0\,(Nh\nu + P_{\nu}^{b}), \tag{81}$$

where G is the gain, $\Delta\nu_0$ is the bandwidth of the amplifier and P_{ν}^{b} is the spectral density of the background radiation. After incoherent transformation, that is to say, at the output of the detector, the spectral density of the fluctuation intensity due to the detected noise is approximately $P_{\text{out}}^2/\Delta\nu_0$. If $\Delta\nu_d < \Delta\nu_0$, where $\Delta\nu_d$ is the detector bandwidth, this corresponds to a mean-square value of order

$$P_{d} = G\,(Nh\nu + P_{\nu}^{b}\ )\sqrt{\Delta\nu_0 \cdot \Delta\nu_d}. \tag{82}$$

Consequently, in detection of a continuous radiation spectrum the minimum detectable spectral density $P_{\nu}^{\min}$ is

$$P_{\nu}^{\min} = (Nh\nu + P_{\nu}^{b}\ )\sqrt{\frac{\Delta\nu_d}{\Delta\nu_0}}. \tag{83}$$

Until recently the sensitivity of optical detectors was limited by this minimum detectable spectral density because available optical sources were incoherent. With the advent of quantum-mechanical oscillators in the optical region, however, monochromatic optical sources have become available and all the techniques that have been used in radio communication, in particular, phase techniques and coherent conversion, can be used in the optical region. The minimum monochromatic power detectable with a quantum-mechanical amplifier is

$$P^{\min} = (Nh\nu + P_{\nu}^{b})\sqrt{\Delta\nu_0\,\Delta\nu_d}. \tag{84}$$

It is evident from these relations that to increase sensitivity one must either reduce the number of modes in the quantum-mechanical amplifier or must couple the resonator in the quantum-mechanical amplifier to the later stages of the receiver in such a way that the minimum possible number of modes is supported.

In the limiting case of low background and N = 1 with $\nu = 10^{14}$ cps, $\Delta\nu_0 = 10^{10}$ cps, and $\Delta\nu_d = 10^3$ cps (bandwidth corresponding to response time of a bolometer), we find $P_{\nu}^{\min} = 10^{-23}$ W/cycle. In the bolometer case the integrated intensity of 10^{-10} W with a bandwidth of 10^{11} cps corresponds to $P_{\nu}^{\min} = 10^{-21}$ W/cycle. Under these same conditions we find that $P^{\min} = 10^{-13}$ W for a quantum-mechanical amplifier used to receive a monochromatic signal.

Thus, the calculations show that under the limiting conditions at $\nu \sim 10^{14}$ cps the sensitivity of the quantum-mechanical amplifier can exceed that of a bolometer.

In this analysis we have neglected additional fluctuations caused by instabilities in the pump radiation in nonsaturation operation. Because there is no information presently available concerning operating quantum-mechanical amplifiers it is difficult to evaluate the degree to which the limiting sensitivity has been approached.

In conclusion, we note that optical quantum-mechanical amplifiers can offer the fundamental advantage of coherent amplification of optical radiation.

3. Quantum counters. Optical quantum-mechanical amplifiers have a relatively high inherent noise level because of spontaneous emission. Devices for detection of infrared radiation, capable of detecting single photons, have been proposed in [3] and [129]. In these devices, the entire population is in the lower level when there is no external signal, so that there is no spontaneous emission noise. The signal causes transitions to an excited level; at this level the pump radiation causes transitions to a still higher level. Transitions from this level to the lower state are accompanied by the emission of an optical photon, which is then detected by a photomultiplier or similar high-sensitivity device, capable of detecting individual photons (Fig. 27). Thus, this device essentially converts infrared photons into photons of higher frequency, at which

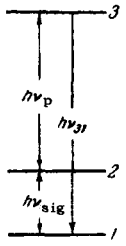

FIG. 27. Quantum counter.

the sensitivity of receiving devices is such that individual photons can be detected.

A paramagnetic crystal can be used in a quantum counter, since the lifetime of the excited state is usually long, 10^{-2}—10^{-3} sec, the time required for transitions to occur will be at least this long.[130] Consequently the time constant of a quantum counter will be at least 10^{-2}—10^{-3} sec. In the general case the time for transition processes is determined by the slowest process in the quantum counter.

In analyzing the sensitivity[77] of a quantum counter we assume that the efficiency of the photodetector $\alpha h\nu_{31} = 1$. In this case the inherent shot noise of the photocell can be neglected. Here, α is the quantum sensitivity of the photo-element and ν_{31} is the frequency at which the signal photons are produced. The spontaneous emission noise in a quantum counter can also be avoided. This means that if a counter is at zero temperature each photon can be detected if there is no external background. If the temperature is nonzero there will be internal noise in the counter. In the presence of an external background the counter temperature must be such that the total noise level is determined by the external radiation background against which the signal is detected. In contrast with the quantum-mechanical amplifier, because of the absence of spontaneous noise in a counter it is possible to reach a sensitivity threshold determined by the background alone.

Under saturation conditions due to the pump transition in a three-level counter the minimum detectable number of photons in a signal is

$$N_s = (N_d + e^{-h\nu/kT}) \sqrt{\frac{\tau_{31}}{\tau_0}} \approx N_b \sqrt{\frac{\tau_{31}}{\tau_0}}, \quad (85)$$

where N_b is the number of background photons, ν is the signal frequency, T is the counter temperature, $\tau_{31} = 1/w_{31}$, while w_{31} is the probability of a spontaneous $3 \rightarrow 1$ transition and τ_0 is the time constant of the photodetector. In the detection of thermal radiation N_S and N_b are related in the same way to the corresponding spectral densities. Hence,

$$P_\nu^{sig} = P_\nu^b \sqrt{\frac{\tau_{31}}{\tau_0}}. \quad (86)$$

In the detection of a monochromatic signal

$$P^{sig} = P_\nu^b \Delta\nu_l \sqrt{\frac{\tau_{31}}{\tau_0}}, \quad (87)$$

if the working material of the counter is in a resonator with a bandwidth $\Delta\nu_0$ larger than the line width of the signal transition $\Delta\nu_l$ and

$$P^{sig} = P_\nu^b \Delta\nu_0 \sqrt{\frac{\tau_{31}}{\tau_0}} \quad (88)$$

if this is not the case. It is evident that the second case is preferable. With $\nu = 10^{14}$ cps, $T_b = 300°K$ and an aperture 1 cm^2, $P_\nu^b = 10^{-20}$ W/cycle while with $T_b = 100°K$, $P_\nu^b = 10^{-35}$ W/cycle, which is appreciably greater than the sensitivity of a quantum-mechanical amplifier.

Because of the lack of information concerning the development of quantum counters it is impossible to say anything about the sensitivity that has been achieved in practice.

VI. CONCLUSION

In the brief period of its existence the field of quantum electronics has already achieved impressive success. Ultra-accurate molecular frequency standards have been built and used for various purposes as have ultra-low-noise microwave paramagnetic amplifiers. Moreover, optical masers have been built and exhibit a high degree of coherence together with a high spectral density.

Various kinds of materials in the gaseous and solid state are used in quantum-mechanical devices but paramagnetic crystals have found the widest application. It is expected that the number of materials used in the future will become greater and greater. New kinds of quantum-mechanical devices will be built and the range of available wavelengths will be extended to the submillimeter and the far infrared.

Optical masers can be useful for space communication, for high-capacity communication channels, in chemistry, biology and so on.

The rapid progress of quantum electronics is due in part to the fact that its development did not require new techniques. Optical masers could have been built 20 years ago, when the condition for producing "negative absorption" of radiation was formulated for the first time.[133] The initial advances were achieved in the microwave region and these were followed by successes in the optical region.

At the present time work is under way to cover the entire range, including the submillimeter and the far infrared. There is little doubt that the range of application of these quantum-mechanical devices will continue to increase.

[1] N. G. Basov and A. M. Prokhorov, UFN **57**, 485 (1955).

[2] N. G. Basov and A. N. Oraevskii, Izv. vuzov (Radiotekhnika) **2**, 3 (1959).

[3] J. Weber, Phys. Rev. **108**, 537 (1957).

[4] J. P. Wittke, Proc. Inst. Radio Engrs. **45**, 291 (1957).
[5] Basov, Krokhin, and Popov, UFN **72**, 161 (1960), Soviet Phys. Uspekhi **3**, 702 (1961).
[6] E. K. Zavoĭskii, Doctoral Dissertation (Physics Institute, Acad. Sci. USSR 1944.
[7] M. H. L. Pryce, Proc. Phys. Soc. (London) **A63**, 25 (1950).
[8] B. Bleaney and K. W. H. Stevens, Repts. Progr. Phys. **16**, 107 (1953).
[9] K. D. Bowers and J. Owen, Repts. Progr. Phys. **18**, 304 (1955).
[10] D. Ingram, Spectroscopy at Radio and Microwave Frequencies, (Russ. Transl.) M., IL, 1959.
[11] W. Low, Paramagnetic Resonance in Solids, Academic Press, New York, 1960.
[12] S. A. Al'tshuler and B. M. Kozyrev, Elektronnyĭ paramagnitnyĭ rezonans (Electronic Paramagnetic Resonance), M., Fizmatgiz, 1961.
[13] J. H. Van Vleck, Phys. Rev. **41**, 208 (1932).
[14] R. Schapp and W. G. Penney, Phys. Rev. **41**, 194 (1932); **42**, 666 (1932).
[15] A. Siegert, Physica **4**, 138 (1937).
[16] S. Sugano and Y. Tanabe, J. Phys. Soc. Japan **13**, 880 (1958).
[17] R. J. Elliot and K. W. H. Stevens, Proc. Phys. Soc. (London) **A64**, 205 (1951); Proc. Roy. Soc. (London) **A219**, 387 (1953).
[18] M. H. L. Pryce and W. A. Runciman, Disc. Faraday Soc. **26**, 34 (1958).
[19] A. A. Manenkov and A. M. Prokhorov, JETP **28**, 762 (1955), Soviet Phys. JETP **1**, 611 (1955).
[20] M. M. Zaripov and Yu. A. Shamonin, JETP **30**, 291 (1956), Soviet Phys. JETP **3**, 171 (1956).
[21] J. E. Geusic, Phys. Rev. **102**, 1252 (1956).
[22] G. M. Zverev and A. M. Prokhorov, JETP **34**, 513 (1958), Soviet Phys. JETP **7**, 354 (1958).
[23] J. E. Geusic and E. O. Shulz-DuBois, Bell Syst. Tech. J. **38**, 271 (1959).
[24] L. S. Kornienko and A. M. Prokhorov, JETP **33**, 805 (1957), Soviet Phys. JETP **6**, 620 (1958).
[25] L. S. Kornienko and A. M. Prokhorov, JETP **36**, 919 (1959), Soviet Phys. JETP **9**, 649 (1959).
[26] G. S. Bogle and H. F. Symmons, Proc. Phys. Soc. (London) **73**, 531 (1959).
[27] L. S. Kornienko and A. M. Prokhorov, JETP **40**, 1594 (1961), Soviet Phys. JETP **13**, 1120 (1961).
[28] Vinokurov, Zaripov, and Yafaev, JETP **37**, 312 (1959), Soviet Phys. JETP **10**, 220 (1960).
[29] F. A. Grant, Revs. Modern Phys. **31**, 646 (1959).
[30] Gerritsen, Harrison, and Lewis, J. Appl. Phys. **31**, 1566 (1960).
[31] D. L. Carter and A. Okaya, Phys. Rev. **118**, 1485 (1960).
[32] Versanyi, Wood, and Shawlow, Phys. Rev. Letters **3**, 544 (1959).
[33] W. Low, Phys. Rev. **118**, 1608 (1960).
[34] J. Waller, Z. Physik **79**, 370 (1932).
[35] R. L. Kronig, Physica **6**, 33 (1939).
[36] J. H. Van Vleck, Phys. Rev. **57**, 426, 1052 (1940).
[37] S. A. Al'tshuler, Izv. AN SSSR, ser. fiz. **20**, 1207 (1956).
[38] S. A. Al'tshuler, JETP **24**, 681 (1953).
[39] V. I. Avvakumov, FMM **4**, 199 (1957).
[40] Sh. Sh. Bashkirov, FMM **6**, 577 (1958).
[41] Sh. Sh. Bashkirov, JETP **34**, 1465 (1958), Soviet Phys. JETP **7**, 1013 (1958).
[42] L. Ya. Shekun, Dissertation, Khar'kov State Univ., 1956.
[43] B. I. Kochelaev, DAN SSSR **131**, 1053 (1960), Soviet Phys. Doklady **5**, 349 (1960).
[44] B. Bolger, Thesis, Amsterdam, 1959.
[45] Bloembergen, Shapiro, Pershan, and Artman, Phys. Rev. **114**, 445 (1959).
[46] U. Kh. Kopvillem, JETP **38**, 151 (1960), Soviet Phys. JETP **11**, 109 (1960).
[47] W. B. Mims and J. D. McGee, Proc. Inst. Radio Engrs. **47**, 2120 (1959).
[48] R. A. Armstrong and A. Szabo, Can. J. Phys. **38**, 1304 (1960).
[49] A. A. Manenkov and A. M. Prokhorov, JETP **42**, 75 (1962), Soviet Phys. JETP **15**, 54 (1962).
[50] S. Shapiro and N. Bloembergen, Phys. Rev. **116**, 1453 (1959).
[51] G. S. Bogle, Proc. Inst. Radio Engrs. **49**, 573 (1961).
[52] N. G. Basov and A. M. Prokhorov, JETP **28**, 249 (1955), Soviet Phys. JETP **1**, 184 (1955).
[53] N. Bloembergen, Phys. Rev. **104**, 324 (1956).
[54] King, Birko, and Makhov, Proc. Inst. Radio Engrs. **47**, 2025 (1959).
[55] A. Szabo, Can. J. Phys. **37**, 1557 (1959).
[56] Kikuchi, Lambe, Makhov, and Terhune, J. Appl. Phys. **30**, 1061 (1959).
[57] T. H. Maiman, J. Appl. Phys. **31**, 222 (1960).
[58] B. Bolger and B. J. Robinson, Physica **26**, 133 (1960).
[59] Scovil, Feher, and Seidel, Phys. Rev. **105**, 762 (1957).
[60] Davis, Strandberg, and Kyhl, Phys. Rev. **111**, 1268 (1958).
[61] K. D. Bowers and W. B. Mims, Phys. Rev. **115**, 285 (1959).
[62] G. M. Zverev and A. M. Prokhorov, JETP **39**, 545 (1960), Soviet Phys. JETP **12**, 382 (1961).
[63] Manenkov, Milyaev, and Prokhorov, FTT **4**, 388 (1962), Soviet Phys. Solid State **4**, 280 (1962).
[64] Giordmaine, Alsop, Nash, and Townes, Phys. Rev. **109**, 302 (1958).
[65] Castle, Chester, and Wagner, Phys. Rev. **119**, 953 (1960).
[66] P. P. Pashinin and A. M. Prokhorov, JETP **40**, 49 (1961), Soviet Phys. JETP **13**, 33 (1961).
[67] N. Bloembergen, Phys. Rev. **109**, 2209 (1958).

[68] A. A. Manenkov and A. M. Prokhorov, JETP **38**, 729 (1960), Soviet Phys. JETP **11**, 527 (1960).
[69] Pace, Sampson, and Thorp, Phys. Rev. Letters **4**, 18 (1960).
[70] A. A. Manenkov and A. M. Prokhorov, JETP **42**, 1371 (1962), Soviet Phys. JETP **15**, 951 (1962).
[71] A. A. Manenkov and V. B. Fedorov, JETP **38**, 1042 (1960), Soviet Phys. JETP **11**, 751 (1960).
[72] M. W. P. Strandberg, Phys. Rev. **110**, 65 (1958).
[73] Pace, Sampson, and Thorp, Proc. Phys. Sci. (London) **77**, 257 (1961).
[74] Gerritsen, Harrison, Lewis, and Wittke, Phys. Rev. Letters **2**, 153 (1959).
[75] Sierro, Muller, and Lacroix, Arch. Sci. (Geneva) **12**, 122 (1959).
[76] Okaya, Carter, and Nash, Bull. Am. Phys. Soc. **11**, 73 (1960).
[77] N. V. Karlov and A. M. Prokhorov, Radiotekhnika i elektronika **7**, 328 (1962).
[78] G. Feher and H. Scovil, Phys. Rev. **105**, 761 (1957).
[79] A. A. Manenkov and V. A. Milyaev, JETP **41**, 100 (1961), Soviet Phys. JETP **14**, 75 (1962).
[80] G. M. Zverev, JETP **40**, 1667 (1961), Soviet Phys. JETP **13**, 1175 (1961).
[81] V. B. Shteinshleger, Radiotekhnika i elektronika **4**, 1947 (1959).
[82] Karlov, Pimenov, and Prokhorov, Radiotekhnika i elektronika **6**, 410 (1961).
[83] R. V. Pound, Ann. Phys. **1**, 24 (1957).
[84] M. W. Muller, Phys. Rev. **106**, 8 (1957).
[85] M. W. P. Strandberg, Phys. Rev. **107**, 1483 (1957).
[86] M. W. P. Strandberg, Phys. Rev. **108**, 1648 (1957).
[87] Shimoda, Takahasi, and Townes, J. Phys. Soc. Japan **12**, 686 (1957).
[88] A. L. McWhorter and F. R. Arams, Proc. Inst. Radio Engrs. **46**, 913 (1958).
[89] H. B. Callen and T. A. Welton, Phys. Rev. **83**, 34 (1951).
[90] L. D. Landau and E. M. Lifshitz, Elektrodinamika sploshnykh sred (Electrodynamics of Continuous Media), M., Gostekhizdat, 1957.
[91] F. V. Bunkin, Izv. Vuzov (Radiofizika) **4**, No. 3, 496 (1961).
[92] Vuylsteke, Elements of Maser Theory, D. van Nostrand, New York, 1960.
[93] Karlov, Pimenov, and Prokhorov, Radiotekhnika i elektronika **6**, 416 (1961).
[94] Giordmaine, Alsop, Mayer, and Townes, Proc. Inst. Radio Engrs. **47**, 1062 (1959).
[95] F. V. Bunkin and N. V. Karlov, JTP **25**, 438 (1955).
[96] DeGrasse, Scovil, and Shulz-DuBois, Bell. Syst. Tech. J. **38**, 2 (1959).
[97] E. G. Solov'ev and E. K. Karlova, Radiotekhnika i elektronika **6**, 406 (1961).
[98] A. L. McWhorter and J. V. Meyer, Phys. Rev. **109**, 312 (1958).
[99] Morris, Kyhl, and Strandberg, Proc. Inst. Radio Engrs. **47**, 81 (1959).
[100] Makhov, Kikuchi, Lambe, and Terhune, Phys. Rev. **109**, 1399 (1958).
[101] Zverev, Kornienko, Manenkov, and Prokhorov, JETP **34**, 1660 (1958), Soviet Phys. JETP **7**, 1141 (1958).
[102] R. H. Kingston, Proc. Inst. Radio Engrs. **46**, 916 (1958).
[103] S. Foner and L. R. Momo, J. Appl. Phys. **31**, 742 (1960).
[104] Karlov, Pimenov, and Prokhorov, Radiotekhnika i elektronika **6**, 846 (1961).
[105] J. V. Jelley and B. F. C. Cooper, Rev. Sci. Instr. **32**, 166 (1961).
[106] Forward, Goodwin, and Kiefer, IRE Wescon Convention Record **3**, 119 (1959).
[107] S. H. Autler and N. McAvoy, Phys. Rev. **110**, 280 (1958).
[108] Chang, Cromock, and Siegman, IRE Wescon Convention Record **3**, 142 (1959).
[109] Artman, Bloembergen, and Shapiro, Phys. Rev. **109**, 1392 (1958).
[110] P. D. Gianino and F. J. Dominik, Proc. Inst. Radio Engrs. **48**, 260 (1960).
[111] S. H. Autler, Rev. Sci. Instr. **31**, 369 (1960).
[112] C. R. Ditchfield and P. A. Forrester, Phys. Rev. Letters **1**, 448 (1958).
[113] A. M. Prokhorov, JETP **34**, 1658 (1958), Soviet Phys. JETP **7**, 1140 (1958).
[114] A. L. Shawlow and C. H. Townes, Phys. Rev. **112**, 1940 (1958).
[115] T. H. Maiman, Phys. Rev. Letters **4**, 564 (1960); Nature **187**, 493 (1960).
[116] Collins, Nelson, Shawlow, Bond, Garrett, and Kaiser, Phys. Rev. Letters **5**, 303 (1960).
[117] P. P. Sorokin and M. J. Stevenson, Phys. Rev. Letters **5**, 557 (1960).
[118] P. P. Sorokin and M. J. Stevenson, IBM J. Research Develop. **5**, 56 (1961).
[119] Javan, Bennett, and Herriott, Phys. Rev. Letters **6**, 106 (1961).
[120] A. I. Barchukov and A. M. Prokhorov, Radiotekhnika i electronika **4**, 2094 (1959).
[121] I. Wieder and L. R. Sarles, Phys. Rev. Letters **6**, 95 (1961).
[122] J. R. Singer and S. Wang, Second International Conference on Quantum Electronics, Berkeley, 1961.
[123] W. G. Wagner and G. Birnbaum, Second International Conference on Quantum Electronics, Berkeley, 1961.
[124] R. W. Hellwarth, Phys. Rev. Letters **6**, 19 (1961).
[125] A. L. Schawlow and G. E. Devlin, Phys. Rev. Letters **6**, 96 (1961).
[126] C. E. Mandenhall and R. W. Wood, Phil. Mag. **30**, 316 (1915).
[127] O. Detschbein, Ann. Physik **14**, 712 (1932); **14**, 828 (1932).
[128] Shawlow, Wood, and Clogston, Phys. Rev. Letters **3**, 271 (1959).

[129] N. Bloembergen, Phys. Rev. Letters 2, 84 (1959).
[130] A. M. Prokhorov, JETP **40**, 1384 (1961), Soviet Phys. JETP **13**, 973 (1961).
[131] L. N. Galkin and P. P. Feofilov, DAN SSSR **114**, 745 (1957), Soviet Phys. Doklady **2**, 255 (1958).
[132] P. P. Feofilov, Opt. i spektr. (Optics and Spectroscopy) **1**, 992 (1956).
[133] V. A. Fabrikant, Tr. VEI (Trans. All-Union Electrotechnical Inst.) **41**, 236, 254 (1940); Doctoral Dissertation (Physics Institute, Acad. Sci., 1939).
[134] P. W. Anderson, Phys. Rev. **114**, 1002 (1959).

Translated by H. Lashinsky